5-2021

Multi-Scale Dynamical Analysis on Circadian Rhythms of *Arabidopsis thaliana*

Yian Xu
Trinity University, annxu1119@gmail.com

Multi-Scale Dynamical Analysis on Circadian Rhythms of *Arabidopsis thaliana*

Yian Xu

A departmental senior thesis submitted to the Department of Physics and Astronomy at Trinity University in partial fulfillment of the requirements for graduation with departmental honors.

April 22, 2021

Thesis Advisor	Department Chair

Michael Soto, AVPAA

Student Agreement

I grant Trinity University (“Institution”), my academic department (“Department”), and the Texas Digital Library ("TDL") the non-exclusive rights to copy, display, perform, distribute and publish the content I submit to this repository (hereafter called "Work") and to make the Work available in any format in perpetuity as part of a TDL, digital preservation program, Institution or Department repository communication or distribution effort.

I understand that once the Work is submitted, a bibliographic citation to the Work can remain visible in perpetuity, even if the Work is updated or removed.

I understand that the Work's copyright owner(s) will continue to own copyright outside these non-exclusive granted rights.

I warrant that:

1) I am the copyright owner of the Work, or
2) I am one of the copyright owners and have permission from the other owners to submit the Work, or
3) My Institution or Department is the copyright owner and I have permission to submit the Work, or
4) Another party is the copyright owner and I have permission to submit the Work.

Based on this, I further warrant to my knowledge:

1) The Work does not infringe any copyright, patent, or trade secrets of any third party,
2) The Work does not contain any libelous matter, nor invade the privacy of any person or third party, and
3) That no right in the Work has been sold, mortgaged, or otherwise disposed of, and is free from all claims.

I agree to hold TDL, DPN, Institution, Department, and their agents harmless for any liability arising from any breach of the above warranties or any claim of intellectual property infringement arising from the exercise of these non-exclusive granted rights.”

I choose the following option for sharing my thesis (required):

[x] Open Access (full-text discoverable via search engines)
[ ] Restricted to campus viewing only (allow access only on the Trinity University campus via digitalcommons.trinity.edu)

I choose to append the following Creative Commons license (optional):

Multi-Scale Dynamical Analysis on Circadian Rhythms of *Arabidopsis thaliana*

by

Yian Xu

An honors thesis submitted to the Department of Physics & Astronomy at

TRINITY UNIVERSITY

in partial fulfillment of the requirements for the
Bachelor of Science in Physics with Honors
May 2021

Accepted by .....
Prof. Kelvin Cheng

Accepted by .....
Prof. Nirav Mehta

Accepted by .....
Prof. David Pooley

Accepted by .....
Prof. Orrin Shindell

Accepted by .....
Prof. Jennifer Steele, Chair

Accepted by .....
Prof. Niescja Turner

Accepted by .....
Prof. Dennis Ugolini

Multi-Scale Dynamical Analysis on Circadian Rhythms of *Arabidopsis thaliana*

by

Yian Xu

Submitted to the Department of Physics & Astronomy
on April 22, 2021, in partial fulfillment of the
requirements for the Bachelor of Science in Physics with Honors

Abstract

Adapting to the 24-hour periodic environment on the Earth, plants have evolved sets of chemical reactions that regulate their circadian rhythms. A number of research groups studying these circadian reactions in the common laboratory plant *Arabidopsis thaliana* have developed eleven, increasingly elaborate, chemical kinetic models based on genetic feedback loops. Each model consists of a system of coupled nonlinear ordinary differential equations. We find these models are all situated near a Hopf bifurcation in parameter space. This suggests that there may be some biological significance corresponding to this mathematical property.

To study the properties of these systems related to the Hopf bifurcation, we first numerically compute the solutions to the kinetic models for *Arabidopsis thaliana*. At the whole plant scale, we perform a weakly nonlinear analysis, the *Reductive Perturbation Method*, on each model near bifurcation to predict the amplitude and frequency of the oscillating concentration of chemical species from the Stuart-Landau amplitude equation. By scaling the numerical frequencies and amplitudes by our theoretical predictions, we show that the solutions to all these models collapse into a universal parameter-free form. Then, we implement Gillespie's *Stochastic Simulation Algorithm* to simulate the system at the single-cell level and account for random fluctuations in molecule numbers. We relate the two approaches and discuss some implications of our results for improving future modeling efforts to ensure that the models are consistent with each other and with the dynamics of the *Arabidopsis thaliana* circadian rhythms. Finally, we comment on the possible biological significance of the models' mathematical features.

Thesis Supervisor: Prof. O. Shindell

Acknowledgments

I would like to thank Professor Shindell for his continual guidance and help on this project over the past four years. Thank you for being patient with me as I not only learn the physics and maths needed for this project but the coding skill as well.

Thank you to the Trinity University Department of Physics and Astronomy, and the Murchison Fellowship for funding support.

Contents

Chapter 1

Circadian Rhythms Networks of *Arabidopsis thaliana*

1.1 Introduction

Adapting to the 24-hour light-dark cycle caused by the rotation of the Earth, plants have evolved genetically regulated chemical reactions to control many of their biological functions [1] called the circadian rhythms network. In the past 16 years, groups of researchers have developed over 11 dynamic models of the circadian rhythms gene network of the plant *Arabidopsis thaliana* [2, 3, 4, 5, 6, 7, 8, 9, 10, 11, 12]. Each of these models are described with a system of first-order, nonlinear, ordinary differential equations (ODEs).

In this thesis, we analyze the dynamics of these models at both the microscopic and macroscopic level. We conduct simulations under perpetual illumination or perpetual darkness to analyze the autonomous version of the models. The autonomous models eliminate the effects of environment changes (light), and show the properties of the circadian rhythms system due to its internal mechanism. The macroscopic approach we take is to use the *Reductive Perturbation Method* by Y. Kuramoto [13]. Ten of the eleven models we study are situated near a Hopf bifurcation, which is the criteria required to apply the *Reductive Perturbation Method* analysis. Using this method, we are able to reduce all ten models into a two-dimensional universal form.

The nonlinear dynamics analysis works well as long as the systems are large, so that the concentration of chemical species can be treated as continuous variables. However, the chemical reactions take place in single plant cells, in which the particle numbers of chemical species can be as small as a few hundred. This is a much smaller system, and any changes in particle numbers can lead to significant change of the state of the system. To account for the fluctuations of molecular population levels at the cellular level, we use the *Stochastic Simulation Algorithm* by D. Gillespie [14]. We show that as the system size increases, the result obtained from *Stochastic Simulation Algorithm* agrees with the numerical solution obtained from the ODEs.

1.2 The Gene Network

In 2005, Locke *et al.* published the first mathematical model of the circadian rhythms network of *Arabidopsis thaliana* in "Modelling genetic networks with noisy and varied experimental data: the circadian clock in *Arabidopsis thaliana* " [2]. This model is a system of seven nonlinear, coupled, first-order, ordinary differential equations that correspond to seven chemical species in the gene network. Molecular experimental data was used to identify the components of the network and to guide the choice of parameter values. The two central genes, the *LATE ELONGATED HYPOCOTY/CIRCADIAN CLOCK ASSOCIATED 1 (LHY/CCA1)* and the *TIMING OF CAB EXPRESSION 1 (TOC1)*, form a negative feedback loop as shown in Figure 1-1. The *LHY/CCA1* gene represses the expression of *TOC1* which in turn activates the expression of *LHY/CCA1*. There are one mRNA and two proteins, in the cytoplasm and nucleus, associated with each of the two genes, denoted with subscriptions m, c, n respectively. Besides these six chemical species, there is also a light-sensitive protein in the model. Let $[L], [T], [P]$ denote the concentrations of LHY/CCA1, TOC1, and the light-dependent protein; the system of equations is

$$\frac{d[L_m]}{dt} = q_1[P_n]\Theta_{light} + \frac{n_1[T_n]^a}{g_1^a + [T_n]^a} - \frac{m_1[L_m]}{k_1 + [L_m]} \tag{1.1}$$

$$\frac{d[L_c]}{dt} = p_1[L_m] - r_1[L_c] + r_2[L_n] - \frac{m_2[L_c]}{k_2 + [L_c]} \tag{1.2}$$

$$\frac{d[L_n]}{dt} = r_1[L_c] - r_2[L_n] - \frac{m_3[L_n]}{k_3 + [L_n]} \tag{1.3}$$

$$\frac{d[T_m]}{dt} = \frac{n_2 g_2^b}{g_2^b + [L_n]^b} - \frac{m_4[T_m]}{k_4 + [T_m]} \tag{1.4}$$

$$\frac{d[T_c]}{dt} = p_2[T_m] - r_3[T_c] + r_4[T_n] - \frac{m_5[T_c]}{k_5 + [T_c]} \tag{1.5}$$

$$\frac{d[L_n]}{dt} = r_3[T_c] - r_4[T_n] - \frac{m_6[T_n]}{k_6 + [T_n]} \tag{1.6}$$

$$\frac{d[P_n]}{dt} = (1 - \Theta_{light})p_3 - \frac{m_7[P_n]}{k_7 + [P_n]} - q_2[P_n]\Theta_{light} \tag{1.7}$$

where

$$\Theta_{light} = \begin{cases} 1, & light \\ 0, & dark \end{cases} \tag{1.8}$$

is the light-dependent term. The rate constants are associated with transcription (n, g), degradation (m, k), translation (p), and protein transport between nucleus and cytoplasm (r).

The later models use the L2005a model as the core and add more details and new gene loops to it, causing the size of the newly developed models to increase. The L2005a model consists of 29 parameters. In 2006, Zeilinger *et al.* discovered the morning and evening "arms" of the circadian rhythms of *Arabidopsis thaliana* [5], and this new model consists of 19 ODEs and 91 parameters. From 2010 to 2013, Pokhilko *et al.* included the *EARLY FLOWERING 4/3 (ELF4/3)* gene group into the network [6, 7, 8], which brought the size of the model to 32 ODEs and 134 parameters. As scientists added more details to the circadian models, the size of the system grew rapidly. However, there is little experimental data available to identify

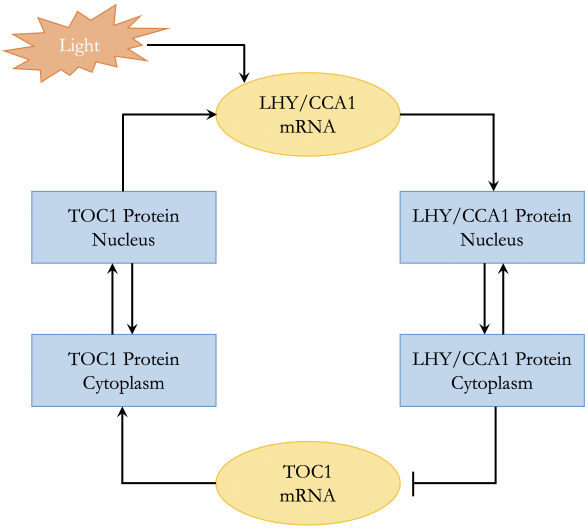

Figure 1-1: Schematic picture of the Locke 2005a circadian rhythms model (L2005a): a two-gene negative feedback loop. [2]

parameter values with precision. The current modeling method uses a search-and-check process to find the optimal parameter values: pick one combination of values from the large set of potential parameter values, then compare the numerical solution of the system with the chosen values to the experimental data, until a cost function that determines the discrepancy between simulation and experimental data is minimized. Such an approach could be time consuming, and potentially unreliable due to the large degrees of freedom. As we describe in later chapters, our analysis using *Reductive Perturbation Method* showed this process of model creation and parameter fitting has yielded models that are dynamically inconsistent with each other.

1.3 Chemical Kinetics

Chemical reactions can be translated into mathematical equations through the *Law of Mass Action* that governs how the rate of reactions depends on chemical concentrations. In open chemical systems, the interaction between the system and its environment plays an important role in the dynamics of the system. One example is the degradation of chemical species. The degradation rates control how fast chemicals leave the system, thus they influence the amount of available chemicals for reactions in the system. Many of the circadian rhythms models, including the L2005a model, use Michaelis–Menten kinetics for enzyme-mediated degradation and Hill functions for the transcription of the mRNAs. In this section, we introduce the *Brusselator*, a toy model illustrating the essential features of oscillatory chemically reacting systems, and we use it to discuss basic ideas of reaction kinetics and *Law of Mass Action*. Then we show how to derive Michaelis–Menten kinetics from the *quasi-steady state hypothesis*, and we discuss the meaning of the Hill function kinetics.

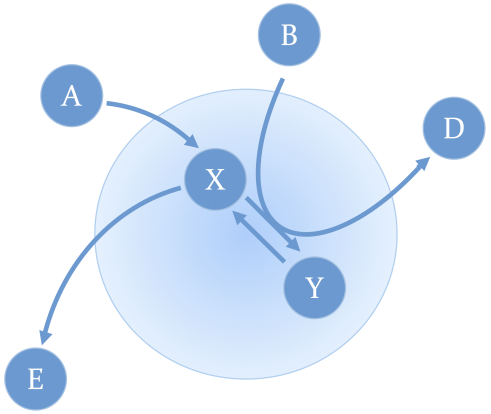

Figure 1-2: The schematic picture of reactions of the Brusselator system. The large circle is the Brusselator system, and X and Y are chemical species that we study. The system is assumed to have infinite source, A and B; and infinite sink, D and E. In the analysis and simulations in this paper, we treat the concentrations of these four source/sink species as constants.

The Brusselator

The *Brusselator* is one of the simplest nonlinear models invented in 1968 and studied by dynamicists at the Brussels school. It is the first known chemical system that shows oscillations while only contains two dependent variables. This two-dimensional hypothetical system has four chemical reactions [15]:

$$A \xrightarrow{k_1} X \tag{1.9}$$

$$2X + Y \xrightarrow{k_2} 3X \tag{1.10}$$

$$B + X \xrightarrow{k_3} Y + D \tag{1.11}$$

$$X \xrightarrow{k_4} E \tag{1.12}$$

where capitalized letters represent chemical species, and k_i are reaction constants. The arrow indicates the direction of reactions. The concentrations of X, Y are the dependent variables, and the concentrations of A, B, D, E are considered as constants. A schematic picture of the Brusselator is shown in Figure 1-2.

Law of Mass Action

The *Law of Mass Action* states that the rate of a reaction is proportional to the product of the concentrations of the reactants. The proportionality constant is called the reaction rate constant. Chemical reactions with more than one reactant require the collision of the reactant molecules which lead to chemical reactions, and the product of concentrations captures the probability of collisions between the reactant molecules. The larger a chemical concentration is, the more molecules there are in unit volume, and the more probable collisions between molecules will occur. We may use the *Law of Mass Action* to translate between chemical reaction equations like Equations 1.9-1.12, and the mathematical description of the model using ODEs. Take the second reaction in the Brusselator (Equation 1.10) as an example,

$$2X + Y \xrightarrow{k_2} 3X$$

This reaction requires a collision between two X molecules and a Y molecule, so the probability of collision is $[X]^2[Y]$, and the reaction rate is $k_2[X]^2[Y]$. Here, we assume that the amounts of X and Y are large enough that their concentrations can be treated as continuous variables. Upon completion of the reaction, the system loses one unit of Y and gains one unit of X. Now the corresponding terms in the differential equations of X and Y are

$$\frac{d[X]}{dt} = \frac{d[X]}{d\,reaction} \cdot \frac{d\,reaction}{dt} = (+1)(k_2[X]^2[Y]) \tag{1.13}$$

$$\frac{d[Y]}{dt} = \frac{d[Y]}{d\,reaction} \cdot \frac{d\,reaction}{dt} = (-1)(k_2[X]^2[Y]) \tag{1.14}$$

where the brackets denote "the concentration of". Applying the same method to all four reactions, the complete set of differential equations of the Brusselator is obtained:

$$\frac{d[X]}{dt} = k_1[A] + k_2[X]^2[Y] - k_3[B][X] - k_4[X] \tag{1.15}$$

$$\frac{d[Y]}{dt} = -k_2[X]^2[Y] + k_3[B][X] \tag{1.16}$$

Michaelis–Menten Kinetics

Many of the circadian rhythms models we study have degradation terms in the form of Michaelis-Menten kinetics. Named after the German Biochemist Leonor Michaelis and Canadian physician Maud Menten, Michaelis-Menten kinetics is one of the most well-known models for chemical systems with an enzyme involved. In this section, we present the enzyme related reactions mathematically, and derive the desired form of the degradation terms using Michaelis-Menten kinetics. The derivations in this section and the next section are adapted from J.D. Murray's *Mathematical Biology* [16].

Consider an enzymatic reaction involving a substrate S reacting with an enzyme E to form a complex SE which then converted into the product P and the enzyme

$$S + E \underset{k_{-1}}{\overset{k_1}{\rightleftharpoons}} SE \xrightarrow{k_2} P + E \tag{1.17}$$

Notice that the enzyme only facilitates the reaction, and its amount is conserved before and after the reaction. By *Law of Mass Action*, the system of differential equations that governs this reaction is

$$\frac{d[S]}{dt} = -k_1[S][E] + k_{-1}[SE] \tag{1.18}$$

$$\frac{d[E]}{dt} = -k_1[S][E] + k_{-1}[SE] + k_2[SE] \tag{1.19}$$

$$\frac{d[SE]}{dt} = k_1[S][E] - k_{-1}[SE] - k_2[SE] \tag{1.20}$$

$$\frac{d[P]}{dt} = k_2[SE] \tag{1.21}$$

Assume that at $t = 0$, the initial conditions of the system are

$$[S](0) = S_0,\ [E](0) = E_0,\ [SE](0) = 0,\ [P](0) = 0. \tag{1.22}$$

At any time $t \geq 0$, the enzyme can take two forms: the free form E, and the bounded form in complex SE. Since the total amount of the enzyme is constant, we have

$$[E] + [SE] = E_0 \tag{1.23}$$

The solution of Equation 1.21 is

$$[P](t) = \int_0^t k_2[SE]dt \tag{1.24}$$

If $[SE](t)$ is known, we could solve $[P](t)$ using the above integral.

Rewriting Equations 1.18–1.21 using Equations 1.23 and 1.24, the system may be reduced to a two-dimensional system

$$\begin{aligned} \frac{d[S]}{dt} &= -k_1[S]\left(E_0 - [SE]\right) + k_{-1}[SE] = -k_1E_0[S] + (k_1[S] + k_{-1})[SE] \\ \frac{d[SE]}{dt} &= k_1[S]\left(E_0 - [SE]\right) - (k_{-1} + k_2)[SE] = k_1E_0[S] - (k_1[S] + k_{-1} + k_2)[SE] \end{aligned} \tag{1.25}$$

with initial conditions $[S](0) = S_0,\ [SE](0) = 0$.

It is convenient to nondimensionalize the system by introducing the following dimensionless quantities

$$\begin{gathered} \tau = k_1E_0t, \quad s(\tau) = \frac{[S](t)}{S_0}, \quad e(\tau) = \frac{[SE](t)}{E_0}, \quad \lambda = \frac{k_2}{k_1S_0}, \quad K = \frac{k_{-1} + k_2}{k_1S_0}, \quad \epsilon = \frac{E_0}{S_0} \\ \Rightarrow \quad d\tau = k_1E_0dt \quad \Rightarrow \quad \frac{d}{dt} = k_1E_0\frac{d}{d\tau} \end{gathered} \tag{1.26}$$

Substituting these quantities into Equations 1.25 gives

$$\begin{aligned} k_1E_0S_0\frac{ds}{d\tau} &= -k_1E_0S_0s + (k_1S_0s + k_{-1})E_0e \\ \Rightarrow \quad \frac{ds}{d\tau} &= -s + \left(s + \frac{k_{-1}}{k_1S_0}\right)e \\ &= -s + \left(s + \frac{k_{-1} + k_2 - k_2}{k_1S_0}\right)e \\ \Rightarrow \quad \frac{ds}{d\tau} &= -s + (s + K - \lambda)\,e \\ k_1E_0^2\frac{de}{d\tau} &= k_1E_0S_0s - (k_1S_0s + k_{-1} + k_2)E_0e \\ \Rightarrow \quad \frac{E_0}{S_0}\frac{de}{d\tau} &= s - \left(s + \frac{k_{-1} + k_2}{k_1S_0}\right)e \\ \Rightarrow \quad \epsilon\frac{de}{d\tau} &= s - (s + K)\,e \end{aligned} \tag{1.27}$$

with initial conditions $s(0) = 1, e(0) = 0$. In most biological systems, the concentration of the substrate is much larger than that of the enzyme, thus, we have $\epsilon \ll 1$, which gives

$$s - (s + K)\,e \approx 0 \tag{1.28}$$

from the last equation in 1.27. This approximation is known as the *quasi-steady state hypothesis*, which

states that the substrate-enzyme reaction happens so much faster that for times of order τ, the reaction is essentially at equilibrium. This quasi-steady state approximation gives

$$e = \frac{s}{K+s} \tag{1.29}$$

which leads to

$$\frac{ds}{d\tau} = -s + (s + K - \lambda)\left(\frac{s}{K+s}\right) = -\frac{\lambda s}{K+s} \tag{1.30}$$

Rewriting in dimensional form, we have

$$\begin{aligned} \frac{d[S]}{k_1 E_0 S_0 dt} &= -\frac{\left(\frac{k_2}{k_1 S_0}\right)\left(\frac{[S]}{S_0}\right)}{\frac{K_m}{S_0} + \frac{[S]}{S_0}}, \qquad K_m = K S_0 \\ \Rightarrow \quad \frac{d[S]}{dt} &= -\frac{(k_2 E_0)[S]}{K_m + [S]} \\ \Rightarrow \quad \frac{d[S]}{dt} &= -\frac{M[S]}{K_m + [S]}, \qquad M = k_2 E_0 \end{aligned} \tag{1.31}$$

which is precisely the form of the degradation terms in the L2005a model.

Hill Functions

In Equations 1.1 and 1.4, the transcription of the mRNAs is described using terms similar to those in Michaelis-Mention kinetics. When an unknown chain of enzymatic reactions is involved, Hill functions are often used, and the Hill coefficients are determined by making a Hill plot of experimental data. The Hill function assumes that the rate of reaction is of the form

$$\frac{d[X]}{dt} = \frac{Q[X]^n}{K + [X]^n}$$

Consider the transcription term of LHY mRNA

$$\frac{d[L_m]}{dt} = \frac{n_1 [T_n]^a}{g_1^a + [T_n]^a},$$

To determine the value of a, the reaction speed $|d[T_m]/dt|_{t=0}$ is measured experimentally with various initial values of $[T_m]$. Let the initial conditions be

$$\frac{d[L_m]}{dt} = R_0, \ [L_m] = L_0, \ [T_n] = T_0$$

The transcription term at $t = 0$ may thus be rewritten as

$$R_0 = \frac{n_1 T_0^a}{g_1^a + T_0^a} \quad \Rightarrow \quad T_0^a = \frac{g_1^a R_0}{n_1 - R_0}$$

$$\Rightarrow a \ln(T_0) = a \ln(g_1) + \ln\left(\frac{R_0}{n_1 - R_0}\right)$$

$$\Rightarrow \ln\left(\frac{R_0}{n_1 - R_0}\right) = a \ln(T_0) - a \ln(g_1)$$

A Hill plot is the graph of $\ln[R_0/(n_1 - R_0)]$ vs. $\ln(T_0)$. Given the value of n_1, the value of a can be obtained from the slope and the intercept of Hill plot.

Chapter 2

Nonlinear Oscillations and Hopf Bifurcation

2.1 Introduction

Sustained oscillations are ubiquitous in living systems. Examples include the cell cycle [17], the respiratory oscillator [18], and the circadian rhythms we study here. Bifurcation is the onset of sustained oscillations as an external parameter is varied. One common type of bifurcation that occurs in oscillating biological systems is the Hopf bifurcation. The amplitude of oscillation of a Hopf bifurcation is proportional to the square root of the bifurcation parameter, and the frequency of oscillation is a linear function of the parameter. Mathematically, Hopf bifurcation is closely related to the eigenvalues of the Jacobian of the system. In this chapter, we introduce the Hopf bifurcation and the properties of the solutions for systems that possess Hopf bifurcations.

2.2 Hopf Bifurcation

The following theory is adapted from *Theory and Applications of Hopf Bifurcation* by B.D. Hassard *et al.* [19]. Consider an autonomous system of nonlinear ordinary differential equations

$$\dot{\mathbf{x}} = \mathbf{f}(\mathbf{x};\mu),\ \mathbf{x} \in \mathbb{R}^n,\ \mathbf{f} : \mathbb{R}^n \to \mathbb{R}^n, \tag{2.1}$$

where μ is a real valued parameter. The Jacobian matrix of the system, $\mathbf{L}$, written in its index notation, is

$$L_{ij}(\mathbf{x},\mu) = \frac{\partial f_i}{\partial x_j}(\mathbf{x},\mu) \quad i,j = 1,2,\ldots,n \tag{2.2}$$

If the system has a fixed point $\mathbf{x} = \mathbf{x}_0$, and the Jacobian evaluated at $\mathbf{x}_0$ has a pair of complex eigenvalues

$$\lambda_+(\mu) = \bar{\lambda}_-(\mu) = \sigma(\mu) + i\omega(\mu) \tag{2.3}$$

such that for some $\mu = \mu_c$,

$$\sigma(\mu_c) = 0,\ \omega(\mu_c) > 0,\ \omega'(\mu_c) \neq 0 \tag{2.4}$$

while other eigenvalues of $\mathbf{L}(\mu_\mathbf{c})$ all have strictly negative real parts, then a Hopf bifurcation occurs, and μ_c is the critical value. There are two kinds of equilibrium existing in Hopf bifurcation: the fixed points, which correspond to constant $\mathbf{x}$ values in time; and the limit cycles, which are sustained oscillations in time. When the system is above bifurcation, the equilibrium contains an unstable fixed point and a stable limit cycle; when the system is below bifurcation, the only equilibrium is a stable fixed point.

The Normal Form and Properties of System Solutions

To study the properties of the system solutions near a Hopf bifurcation, we consider the simplest system that possesses a Hopf bifurcation: a two-dimensional system that possesses a Hopf bifurcation at bifurcation parameter $\mu = 0$. In this section, we derive the normal form of Hopf bifurcation from this system, from which generic scaling properties of the limit cycle oscillations could be found. Details to this derivation may be found in Chapter 8 of paper "Bifurcation Analysis of Non-linear Differential Equations" by C. McCann [20]. The two-dimensional system

$$\begin{aligned} \frac{dx_1}{dt} &= f(x_1, x_2, \mu) \\ \frac{dx_2}{dt} &= g(x_1, x_2, \mu) \end{aligned} \tag{2.5}$$

is assumed to have equilibrium $\mathbf{x}_0 = (0, 0)$, and the eigenvalues of the linearized system are $\lambda_\pm = \alpha(\mu) \pm i\beta(\mu)$. The real parts of the eigenvalues are zero at $\mu = 0$. Now we have

$$f(0, 0, \mu) = g(0, 0, \mu) = 0, \quad \alpha(0) = 0 \tag{2.6}$$

The Maclaurin series expansion of the system around criticality is

$$\begin{aligned} \frac{dx_1}{dt} &= f(0,0,\mu) + x_1\frac{\partial f}{\partial x_1}(0,0) + x_2\frac{\partial f}{\partial x_2}(0,0) + \frac{x_1^2}{2}\frac{\partial^2 f}{\partial x_1^2}(0,0) + x_1x_2\frac{\partial^2 f}{\partial x_1 \partial x_2}(0,0) + \frac{x_2^2}{2}\frac{\partial^2 f}{\partial x_2^2}(0,0) + \cdots \\ &= x_1\frac{\partial f}{\partial x_1}(0,0) + x_2\frac{\partial f}{\partial x_2}(0,0) + f_2(x_1, x_2, \mu), \qquad f_2 = \text{second and higher order terms} \\ \frac{dx_2}{dt} &= g(0,0,\mu) + x_1\frac{\partial g}{\partial x_1}(0,0) + x_2\frac{\partial g}{\partial x_2}(0,0) + \frac{x_1^2}{2}\frac{\partial^2 g}{\partial x_1^2}(0,0) + x_1x_2\frac{\partial^2 g}{\partial x_1 \partial x_2}(0,0) + \frac{x_2^2}{2}\frac{\partial^2 g}{\partial x_2^2}(0,0) + \cdots \\ &= x_1\frac{\partial g}{\partial x_1}(0,0) + x_2\frac{\partial g}{\partial x_2}(0,0) + g_2(x_1, x_2, \mu), \qquad g_2 = \text{second and higher order terms} \end{aligned} \tag{2.7}$$

It may be shown that a 2×2 real-valued matrix A with complex eigenvalues $\lambda_\pm = \alpha \pm i\beta$ and corresponding eigenvectors $\mathbf{v}_\pm = \mathbf{v}_{\pm,r} + i\mathbf{v}_{\pm,i}$ has canonical decomposition $A = TNT^{-1}$, where $T = \begin{pmatrix} v_{+,r} & v_{+,i} \\ v_{-,r} & v_{-,i} \end{pmatrix}$, and $N = \begin{pmatrix} \alpha & -\beta \\ \beta & \alpha \end{pmatrix}$. Applying this result to Equation 2.7, the system can be transformed into its Jordan

normal form

$$\begin{aligned}\frac{du}{dt} &= \alpha(\mu)u - \beta(\mu)v + F_2(u,v,\mu)\\ \frac{dv}{dt} &= \beta(\mu)u + \alpha(\mu)v + G_2(u,v,\mu)\end{aligned} \tag{2.8}$$

We define a complex number $z = u + iv$ and its complex conjugate, now $u = (z+\overline{z})/2$ and $v = (z-\overline{z})/2i$. Substituting the expression in terms of z and $\overline{z}$ for u and v gives

$$\begin{aligned}\frac{1}{2}\frac{d(z+\overline{z})}{dt} &= \alpha(\mu)\frac{(z+\overline{z})}{2} - \beta(\mu)\frac{(z-\overline{z})}{2i} + F_2(z,\overline{z},\mu)\\ \frac{1}{2i}\frac{d(z-\overline{z})}{dt} &= \beta(\mu)\frac{(z+\overline{z})}{2} + \alpha(\mu)\frac{(z-\overline{z})}{2i} + G_2(z,\overline{z},\mu)\end{aligned} \tag{2.9}$$

Multiplying the second equation by i, then adding the resulting equation to the first equation in 2.9, the linear combination gives

$$\begin{aligned}&\frac{dz}{dt} = \alpha z + i\beta z + F_2 + iG_2\\ &\Rightarrow \dot{z} = \lambda_+ z + F(z,\overline{z},\mu), \qquad F = F_2 + iG_2\end{aligned} \tag{2.10}$$

It may be shown that the higher order terms of z only and $\overline{z}$ only contained in F can be eliminated with appropriate form of z. Equation 2.10 can be reduced to the form

$$\dot{w} = \lambda_+ w + \delta w^2 \overline{w} \tag{2.11}$$

where w and δ are complex numbers. Let $w = \rho e^{i\phi}, \delta = c + id$, and recall that $\lambda_+ = \alpha + i\beta$, we can obtain two differential equations by equating the real and imaginary parts of Equation 2.11 separately:

$$\begin{aligned}\dot{\rho}e^{i\phi} + \rho e^{i\phi}(i\dot{\phi}) &= (c+id)\rho^3 e^{i\phi} + (\alpha + i\beta)\rho e^{i\phi}\\ \dot{\rho} + i\rho\dot{\phi} &= c\rho^3 + id\rho^3 + \alpha\rho + i\beta\rho\end{aligned} \tag{2.12}$$

$$\begin{aligned}\Rightarrow \quad \dot{\rho} &= \alpha\rho + c\rho^3\\ \dot{\phi} &= \beta + d\rho^2\end{aligned} \tag{2.13}$$

The first equation in 2.13 tells us about the amplitude of the oscillation, while the second tells about its frequency. To find fixed points and the radius of the limit cycle, we set $\dot{\rho} = 0$, which gives $\rho^* = 0, \pm\sqrt{\gamma}$ where $\gamma = \left|\frac{\alpha}{c}\right|$. Meanwhile, the frequency of the limit cycle is $\dot{\phi}^* = \beta + d\gamma$. Notice that the radius of the limit cycle, or the amplitude of sustained oscillation, is proportional to the square root of the deviation of bifurcation parameter from criticality, while the frequency of the limit cycle scales linearly with the deviation of the bifurcation parameter from criticality.

2.3 Example: the Brusselator

In this section, we use the Brusselator as an example to demonstrate how to calculate the critical value of the bifurcation parameter analytically and various features of Hopf bifurcation described in the previous sections. The Brusselator is described by chemical reactions in Equations 1.9 - 1.12 and in Figure 1-2. Recall that the differential equations governing the Brusselator are given as

$$\begin{aligned} \frac{d[X]}{dt} &= k_1[A] + k_2[X]^2[Y] - k_3[B][X] - k_4[X] \\ \frac{d[Y]}{dt} &= -k_2[X]^2[Y] + k_3[B][X] \end{aligned} \tag{2.14}$$

where $[X]$ and $[Y]$ are the concentrations of species X and Y respectively, and $[A]$ and $[B]$ are constants that represent chemical concentrations of species A and B as the source of the system. Let values of k_i be 1, and $\mathbf{x} = ([X], [Y])^T$. The bifurcation parameter we use here is the concentration of B. The Jacobian of the system is

$$\mathbf{L}(\mathbf{x}, [B]) = \begin{pmatrix} 2[X][Y] - [B] - 1 & [X]^2 \\ [B] - 2[X][Y] & -[X]^2 \end{pmatrix} \tag{2.15}$$

The fixed point $\mathbf{x}_0 = (X_0, Y_0)$ satisfies,

$$\begin{aligned} 0 &= [A] + X_0^2 Y_0 - [B]X_0 - X_0 \\ 0 &= -X_0^2 Y_0 + [B]X_0 \end{aligned} \tag{2.16}$$

Solving the system of equations above gives

$$\mathbf{x}_0 = \begin{pmatrix} [A] \\ {}^{[B]}/_{[A]} \end{pmatrix} \tag{2.17}$$

At the fixed point, $\mathbf{x}$, the Jacobian is

$$\mathbf{L}(\mathbf{x}_0, [B]) = \begin{pmatrix} [B] - 1 & [A]^2 \\ -[B] & -[A]^2 \end{pmatrix} \tag{2.18}$$

with characteristic equation

$$\begin{aligned} &-\left([B] - 1 - \lambda\right)\left([A]^2 + \lambda\right) + [A]^2[B] = 0 \\ \Rightarrow \quad &\lambda^2 + \left(1 - [B] + [A]^2\right)\lambda + [A]^2 = 0 \end{aligned} \tag{2.19}$$

The eigenvalues of the Jacobian can be obtained by solving the characteristic equation:

$$2\lambda_\pm = \left([B] - [A]^2 - 1\right) \pm i\sqrt{4[A]^2 - \left([B] - [A]^2 - 1\right)^2} \tag{2.20}$$

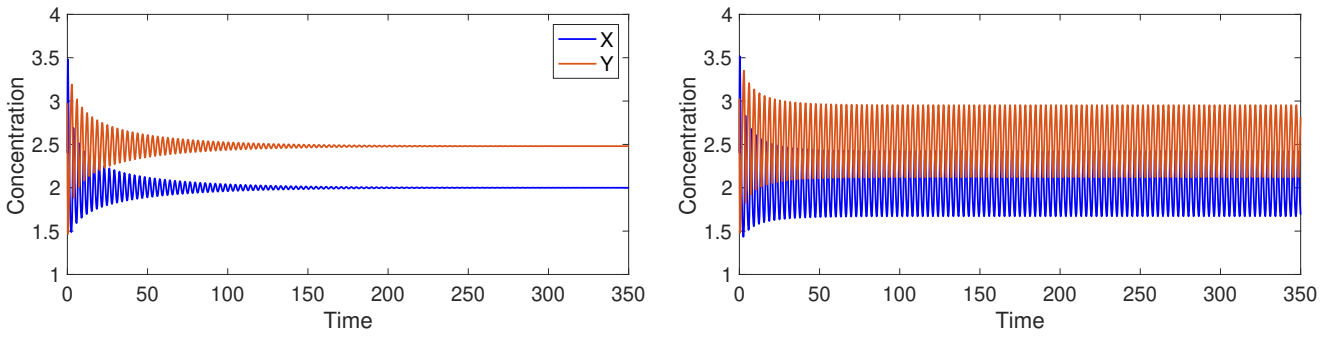

Figure 2-1: Time series plots of the Brusselator with (a) $[B] = 4.96$ and (b) $[B] = 5.05$, which represents subcritical and supercritical oscillations, respectively. $[A] = 2$.

The linearized system exhibits oscillations when imaginary part of the eigenvalues is non-zero in Equation 2.20, that is, the value under the radical is positive:

$$\begin{gathered} 4[A]^2 - ([B]-[A]^2-1)^2 > 0 \\ 2[A] > [B] - [A]^2 - 1 \quad \textit{and} \quad -2[A] < [B] - [A]^2 - 1 \\ [B] < [A]^2 + 2[A] + 1 = \Big([A]^2+1\Big)^2 \quad \textit{and} \quad [B] > [A]^2 - 2[A] + 1 = \Big([A]^2-1\Big)^2 \end{gathered} \tag{2.21}$$

$$\Rightarrow \quad \Big([A]^2-1\Big)^2 < [B] < \Big([A]^2+1\Big)^2 \tag{2.22}$$

The system exhibits growing oscillations when the real part of the eigenvalue is positive, namely,

$$\Big([A]^2+1\Big) < [B] < \Big([A]^2+1\Big)^2 \tag{2.23}$$

and decaying oscillations otherwise. This is because the real part of the eigenvalue defines the envelope of the oscillation for small amplitudes. Let $[A] = 2$, a Hopf bifurcation occurs at $[B] = [A]^2+1 = 5$. Figure 2-1 shows the time series for the Brusselator for both subcritical and supercritical cases with the concentration of A equal to 2. The Brusselator exhibits decaying oscillation and fixed point for $[B] < 5$ (subcritical), and initially growing oscillation that reaches a sustained oscillation for $[B] > 5$ (supercritical). Figure 2-2 shows bifurcation diagrams of the concentration of X and the frequency of oscillation near bifurcation, which confirm that the calculated critical value, $[B]^* = 5$, is correct. The bifurcation diagrams verify that the amplitude of oscillation is proportional to the square root of the distance from bifurcation, and the frequency has a linear relationship with the distance from bifurcation.

2.4 Hopf Bifurcation in the Circadian Rhythms Model

To study the intrinsic mechanisms of the circadian rhythms in *Arabidopsis thaliana*, we set Θ_{light} in the L2005a model to be unity, so the plant is an autonomous system under perpetual illumination. In this section, we use the *LHY* transcription rate (n_1) as the bifurcation parameter. Transcription is the process in the cell's nucleus of copying information from DNA molecule into messenger RNA. Therefore, the

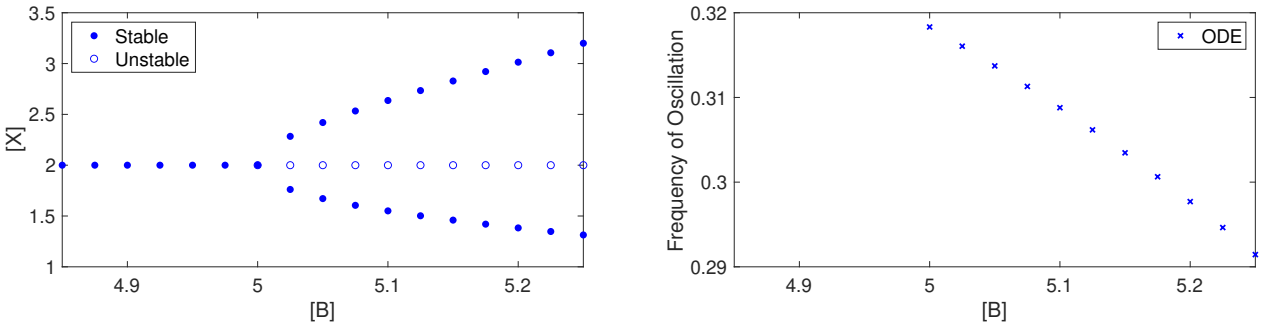

(a) (b)

Figure 2-2: Bifurcation diagrams of (a) concentration of X and (b) oscillatory frequency in the Brusselator model poised near a supercritical Hopf bifurcation. The concentration of A is 2, and bifurcation occurs at $[B] = [A]^2 + 1 = 5$. (a) The central branch is the fixed point, which is stable to the left of criticality (closed circles) and unstable to the right (open circles). The upper and lower branches are the maximum and minimum values of X limit cycle oscillations, calculated numerically (closed blue circles). (b) The limit cycle frequency is calculated numerically (blue cross marks).

transcription rate controls the production of messenger RNA, making it closely relate to the concentration of *LHY* mRNA (L_m) in the circadian model of *Arabidopsis thaliana*.

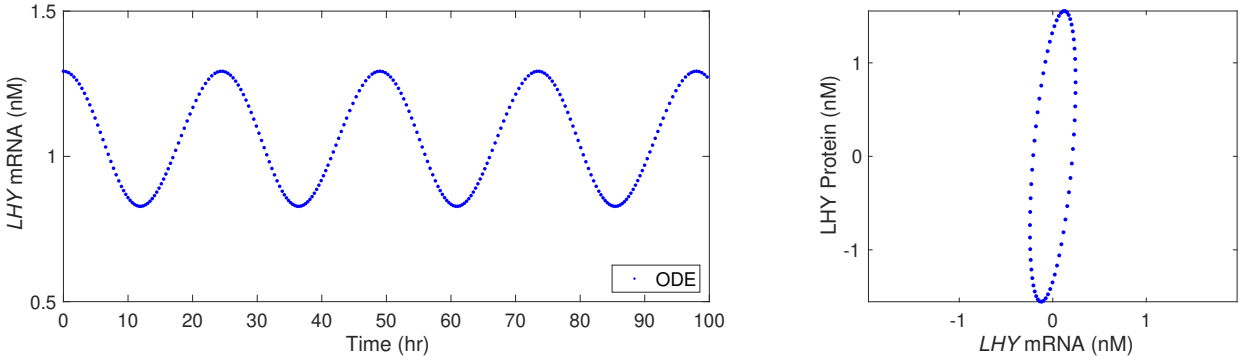

(a) (b)

Figure 2-3: (a) Time series and (b) phase space plot are calculated numerically (ODE) for the L2005a model poised near a supercritical Hopf bifurcation under perpetual illumination.

Figure 2-3 shows the time series of *LHY* mRNA and a phase diagram of Locke *et al.* 2005a model. The signals are numerical solutions to the L2005a ODEs at typical reaction rates, numerically integrated with the MATLAB ODE15s solver [21]. The model displays sustained oscillations at this set of parameter values. In Figure 2-4, we show the bifurcation diagrams of the chemical concentration of *LHY* mRNA and the oscillatory frequency of the L2005a model. The parameter is scaled such that normalized transcription rate of unity corresponds to the biological value. We found the critical value of the normalized transcription rate to be 0.9785 by tracing the eigenvalues of the Jacobian as we vary the normalized transcription rate, and finding the bifurcation parameter value that gives eigenvalues in the form described in Equation 2.4. The bifurcation diagram of concentration shows that the system possesses a Hopf bifurcation, as the system shows a transition from a stable fixed point on the left side of 0.9785, to an unstable fixed point and a stable limit cycle on the right side of 0.9785.

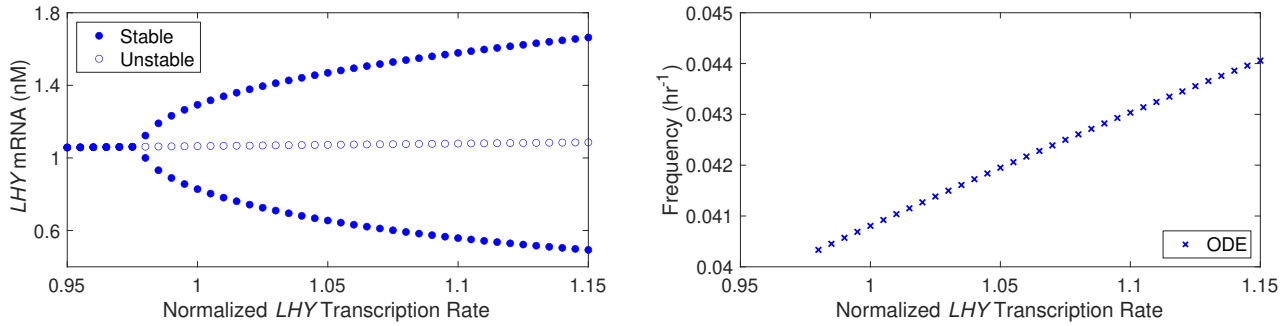

(a) (b)

Figure 2-4: Bifurcation diagrams of (a) chemical concentration of LHY mRNA and (b) oscillatory frequency of circadian rhythms model (L2005a) under perpetual illumination. The transcription rate of LHY is normalized such that the estimated biological value is unity; the bifurcation occurs at 0.9785. (a) The central branch is the fixed point, which is stable to the left of criticality (closed circles) and unstable to the right (open circles). The upper and lower branches are the maximum and minimum values of LHY mRNA limit cycle oscillations, calculated numerically (closed blue circles). (b) The limit cycle frequency is calculated numerically (blue cross marks).

Chapter 3

Reductive Perturbation Method

After applying the bifurcation analysis from the previous chapter to all eleven models, we found that ten of the eleven circadian rhythms models for *Arabidopsis thaliana* are situated near a Hopf bifurcation point, with the exception of the Locke *et al.* 2006 model [4]. The Locke 2006 model shows two pairs of complex eigenvalues with positive real parts, as oppose to one pair for Hopf bifurcation. Small-amplitude oscillations near a Hopf bifurcation can be approximated using the Stuart-Landau equation, which reduces the dynamics of the high dimensional models to a two-dimensional subspace. In this chapter, we show the steps leading to the Stuart-Landau equation directly from the circadian rhythms models, and we show that the *Reductive Perturbation Method* successfully captures dynamical properties of the circadian rhythms models. The following derivation is adapted from *Chemical Oscillations, Waves, and Turbulence* by Y. Kuramoto [13].

3.1 Stuart-Landau Equation

Consider the system described in Equation 2.1,

$$\frac{d\mathbf{x}}{dt} = \mathbf{f}(\mathbf{x};\mu),\ \mathbf{x} \in \mathbb{R}^n,\ \mathbf{f} : \mathbb{R}^n \to \mathbb{R}^n,\ \mathbf{f}(\mathbf{x}_0(\mu);\mu) = 0 \tag{3.1}$$

Without loss of generality, suppose the system possesses a Hopf bifurcation at $\mu = 0$, and $\mu > 0$ means the system is supercritical where it exhibits sustained oscillations. It is more convenient to express the system in terms of $\mathbf{u} \equiv \mathbf{x} - \mathbf{x}_0$, the deviation from the fixed point. The Taylor expansion of the system about $\mathbf{u} = \mathbf{0}$ is then

$$\frac{d\mathbf{u}}{dt} = L\mathbf{u} + M\mathbf{uu} + N\mathbf{uuu} + \cdots \tag{3.2}$$

where L is the Jacobian matrix, M is an array with three indices of mixed partials, and N with four

$$\begin{aligned}(L\mathbf{u})_i &= \sum_j \left.\frac{\partial f_i}{\partial x_j}\right|_{\mathbf{x}_0} u_j \\ (M\mathbf{uu})_i &= \sum_{j,k} \frac{1}{2!} \left.\frac{\partial^2 f_i}{\partial x_j \partial x_k}\right|_{\mathbf{x}_0} u_j u_k \\ (N\mathbf{uuu})_i &= \sum_{j,k,l} \frac{1}{3!} \left.\frac{\partial^3 f_i}{\partial x_j \partial x_k \partial x_l}\right|_{\mathbf{x}_0} u_j u_k u_l\end{aligned} \tag{3.3}$$

According to the definitions, $M\mathbf{uu}$ and $N\mathbf{uuu}$ are symmetric arrays with respect to the i, j, k indices such that their order can be changed, that is, the $\mathbf{u}$'s in Equation 3.3 are commutative.

System Expansions

The solution to Equation 3.2 can be written as a power series

$$\mathbf{u} = \mu^{1/2}\mathbf{u}_1 + \mu\mathbf{u}_2 + \mu^{3/2}\mathbf{u}_3 + \cdots \tag{3.4}$$

where we note again that to lowest order $\mathbf{u} \sim \sqrt{\mu}$. The expansion coefficients L, M, N depend on μ as $\mathbf{x}_0$ has μ dependency. So we expand them into Taylor series about $\mu = 0$ in terms of $\varepsilon^2 \equiv \mu$ for algebraic simplicity

$$\begin{aligned}\mathbf{u} &= \varepsilon\mathbf{u}_1 + \varepsilon^2\mathbf{u}_2 + \varepsilon^3\mathbf{u}_3 + \cdots \\ L &= L_0 + \mu L_1 + \mu^2 L_2 + \cdots = L_0 + \varepsilon^2 L_1 + \cdots \\ M &= M_0 + \mu M_1 + \mu^2 M_2 + \cdots = M_0 + \varepsilon^2 M_1 + \cdots \\ N &= N_0 + \mu N_1 + \mu^2 N_2 + \cdots = N_0 + \varepsilon^2 N_1 + \cdots\end{aligned} \tag{3.5}$$

The L_0, M_0, N_0 are L, M, N evaluated at criticality ($\mu = \mu^* = 0$). The eigenvalues, λ and $\overline{\lambda}$, of the Jacobian satisfy

$$L\mathbf{v} = \lambda\mathbf{v},\ L\overline{\mathbf{v}} = \overline{\lambda}\overline{\mathbf{v}} \quad \mathbf{v}^*L = \lambda\mathbf{v}^*,\ \overline{\mathbf{v}}^*L = \overline{\lambda}\overline{\mathbf{v}}^* \tag{3.6}$$

where $\mathbf{v}$ and $\mathbf{v}^*$ are the right and left eigenvectors, respectively. Note that for $\lambda \neq 0$, if $\mathbf{v}$ and $\mathbf{v}^*$ are normalized such that $\mathbf{v}^*\mathbf{v} = 1$, we have

$$\mathbf{v}^*L\mathbf{v} = \mathbf{v}^*(L\mathbf{v}) = \mathbf{v}^*\lambda\mathbf{v} = \lambda\mathbf{v}^*\mathbf{v} \quad \Rightarrow \quad \mathbf{v}^*L\mathbf{v} = \lambda \tag{3.7}$$

This relationship holds true for the complex conjugates as well. With a Taylor series expansion of λ about $\mu = 0$, Equation 3.7 becomes

$$\left(\mathbf{v}_0^* + \varepsilon^2\mathbf{v}_1^* + \cdots\right)\left(L_0 + \varepsilon^2 L_1 + \cdots\right)\left(\mathbf{v}_0 + \varepsilon^2\mathbf{v}_1 + \cdots\right) = \left(\lambda_0 + \varepsilon^2\lambda_1 + \cdots\right) \tag{3.8}$$

Equating terms with same order of ε gives

$$\begin{aligned} O(1) \quad &: \quad \mathbf{v}_0^* L_0 \mathbf{v}_0 = \lambda_0 \equiv i\omega_0 \\ O(\varepsilon^2) \quad &: \quad \mathbf{v}_0^* L_1 \mathbf{v}_0 + \mathbf{v}_1^* L_0 \mathbf{v}_0 + \mathbf{v}_0^* L_0 \mathbf{v}_1 = \lambda_1 \end{aligned} \tag{3.9}$$

In the order of ε^2 equation

$$\mathbf{v}_1^* \mathbf{L}_0 \mathbf{v}_0 = \mathbf{v}_1^* \lambda_0 \mathbf{v}_0 = \lambda_0 \mathbf{v}_1^* \mathbf{v}_0 \tag{3.10}$$

$$\mathbf{v}_0^* \mathbf{L}_0 \mathbf{v}_1 = \lambda_0^* \mathbf{v}_0^* \mathbf{v}_1 = \left(\lambda_0 \mathbf{v}_1^* \mathbf{v}_0\right)^* \tag{3.11}$$

thus

$$\begin{aligned} & \mathbf{v}_1^* L_0 \mathbf{v}_0 + \mathbf{v}_0^* L_0 \mathbf{v}_1 = 0 \\ \Rightarrow \quad & \mathbf{v}_0^* L_1 \mathbf{v}_0 = \lambda_1 \equiv \sigma_1 + i\omega_1 \end{aligned} \tag{3.12}$$

So, λ_1 may be found from the first-order approximation of the Jacobian matrix evaluated with the normalized eigenvectors of the Jacobian at criticality.

Two-timing and Solution to the System

Notice that λ has real part of order ε^2, which is small, so we introduce a scaled time $\tau = \mu t = \varepsilon^2 t$. Assume the solution to system 3.2, $\mathbf{u}$, depends on both t and τ. Treating t and τ as independent variables, the total time derivative becomes

$$\frac{d}{dt} = \frac{\partial}{\partial t} + \frac{\partial \tau}{\partial t}\frac{\partial}{\partial \tau} = \frac{\partial}{\partial t} + \varepsilon^2 \frac{\partial}{\partial \tau} \tag{3.13}$$

For the sake of simpler notations, we use $\partial/\partial t = \partial_t$ and $\partial/\partial \tau = \partial_\tau$. Now substituting Equations 3.5 and the new time derivative into 3.2 gives

$$(\partial_t + \varepsilon^2 \partial \tau)\mathbf{u} = (L_0 + \varepsilon^2 L_1 + \cdots)\mathbf{u} + (M_0 + \varepsilon^2 M_1 + \cdots)\mathbf{uu} + (N_0 + \varepsilon^2 N_1 + \cdots)\mathbf{uuu} \tag{3.14}$$

Plugging in $\mathbf{u} = \varepsilon \mathbf{u}_1 + \varepsilon^2 \mathbf{u}_2 + \cdots$ and equating the left-hand side (LHS) and the right-hand side (RHS) for orders of ε

$$\begin{aligned} O(\varepsilon) \quad &: \quad \partial_t \mathbf{u}_1 = L_0 \mathbf{u}_1 \\ O(\varepsilon^2) \quad &: \quad \partial_t \mathbf{u}_2 = L_0 \mathbf{u}_2 + M_0 \mathbf{u}_1 \mathbf{u}_1 \\ O(\varepsilon^3) \quad &: \quad \partial_t \mathbf{u}_3 + \partial_\tau \mathbf{u}_1 = L_0 \mathbf{u}_3 + L_1 \mathbf{u}_1 + 2M_0 \mathbf{u}_1 \mathbf{u}_2 + N_0 \mathbf{u}_1 \mathbf{u}_1 \mathbf{u}_1 \end{aligned} \tag{3.15}$$

$$\begin{aligned} & O(\varepsilon) \quad : (\partial_t - L_0)\mathbf{u}_1 = 0 \\ \Rightarrow \quad & O(\varepsilon^2) \quad : (\partial_t - L_0)\mathbf{u}_2 = M_0 \mathbf{u}_1 \mathbf{u}_1 \\ & O(\varepsilon^3) \quad : (\partial_t - L_0)\mathbf{u}_3 = (L_1 - \partial_\tau)\mathbf{u}_1 + 2M_0 \mathbf{u}_1 \mathbf{u}_2 + N_0 \mathbf{u}_1 \mathbf{u}_1 \mathbf{u}_1 \end{aligned} \tag{3.16}$$

From these equations, we conclude that every $\mathbf{u}_i$ is in terms of lower order $\mathbf{u}_i$'s. Therefore, if $\mathbf{u}_1$ is known, so are the higher order $\mathbf{u}_i$. From the $O(\varepsilon)$ equation, $\mathbf{u}_1$ has trivial solution as a linear combination of exponential terms

$$\mathbf{u}_1 = c_1 \mathbf{v}_1 e^{\lambda_1 t} + c_2 \mathbf{v}_1 e^{\lambda_2 t} + \cdots \tag{3.17}$$

where $\mathbf{v}$ are eigenvectors of L_0 with corresponding eigenvalues λ. As time progresses, the behavior of the solution is dominated by the eigenvalues with the largest real part, that is, the pair of eigenvalues that have zero real parts at $\mu = 0$. Label them as $\lambda_\pm = \pm i\omega_0$, $\mathbf{u}_1$ can be estimated as

$$\mathbf{u}_1 \approx c\mathbf{v}_0 e^{i\omega_0 t} + \bar{c}\,\overline{\mathbf{v}}_0 e^{-i\omega_0 t} \tag{3.18}$$

The solution $\mathbf{u}_1$ has both t and τ dependency, so the coefficients c and $\bar{c}$ may have τ dependency. Let $c \equiv W(\tau)$, and the solution becomes

$$\mathbf{u}_1 = W(\tau)\mathbf{v}_0 e^{i\omega_0 t} + \overline{W}(\tau)\overline{\mathbf{v}}_0 e^{-i\omega_0 t} \tag{3.19}$$

Inserting $\mathbf{u}_1$ into the $O(\varepsilon^2)$ equation in 3.16 gives

$$\begin{aligned}(\partial_t - L_0)\mathbf{u}_2 &= M_0\left[W(\tau)\mathbf{v}_0 e^{i\omega_0 t} + \overline{W}(\tau)\overline{\mathbf{v}}_0 e^{-i\omega_0 t}\right]^2 \\ &= M_0\left[W^2\mathbf{v}_0\mathbf{v}_0 e^{2i\omega_0 t} + 2W\overline{W}\mathbf{v}_0\overline{\mathbf{v}}_0 + \overline{W}^2\overline{\mathbf{v}}_0\overline{\mathbf{v}}_0 e^{-2i\omega_0 t}\right]\end{aligned} \tag{3.20}$$

Notice that the RHS of the above equation consists of only the zeroth and second harmonics. We consider the form of $\mathbf{u}_2$ to be

$$\mathbf{u}_2 = W^2 A_+ e^{2i\omega_0 t} + |W|^2 A_0 + \overline{W}^2 A_- e^{-2i\omega_0 t} \tag{3.21}$$

Plugging $\mathbf{u}_2$ into Equation 3.20 and equating the coefficients of the exponential terms in the LHS and RHS, we get

$$\begin{aligned}A_+ &= (2i\omega_0 I - L_0)^{-1} M_0 \mathbf{v}_0\mathbf{v}_0 \\ A_- &= (-2i\omega_0 I - L_0)^{-1} M_0 \overline{\mathbf{v}}_0\overline{\mathbf{v}}_0 \\ A_0 &= -2L_0^{-1} M_0 \mathbf{v}_0\overline{\mathbf{v}}_0\end{aligned} \tag{3.22}$$

where I is the identity matrix with appropriate size. For our purposes, the iterative solution to $\mathbf{u}_3$ is not useful, however the derivative $\partial_\tau W$, the target of our method, is present in the right-hand side of the $O(\varepsilon^3)$ term in Equation 3.16. This we address in the next section.

Solvability Condition

The right-hand side of $O(\varepsilon^3)$ in Equation 3.16 is

$$\begin{aligned}&(L_1 - \partial_\tau)(W\mathbf{v}e^{i\omega_0 t} + c.c.) \\ &+ 2M_0(W\mathbf{v}e^{i\omega_0 t} + c.c.)\left[W^2 A_+ e^{2i\omega_0 t} + |W|^2 A_0 + \overline{W}^2 A_- e^{-2i\omega_0 t} + a_0(W\mathbf{v}e^{i\omega_0 t} + c.c.)\right] \\ &+ N_0(W\mathbf{v}e^{i\omega_0 t} + c.c.)^3 \\ =& \left[W^3(2M_0\mathbf{v}A_+ + N_0\mathbf{v}\mathbf{v}\mathbf{v})e^{3i\omega_0 t} + c.c.\right] + \left[2W^2 a_0 M_0 \mathbf{v}\mathbf{v}e^{2i\omega t} + c.c.\right] \\ &+ \left\{\left[WL_1\mathbf{v} + |W|^2 W[2M_0(\mathbf{v}A_0 + \overline{\mathbf{v}}A_+) + 3N_0\mathbf{v}\mathbf{v}\overline{\mathbf{v}}] - \partial_\tau W\mathbf{v}\right]e^{i\omega_0 t} + c.c.\right\} \\ &+ 4|W|^2 a_0 M_0 \mathbf{v}\overline{\mathbf{v}}\end{aligned} \tag{3.23}$$

In Equation 3.23, only the $e^{\pm i\omega_0 t}$ terms contain information about the τ dependency of W. Therefore, we consider only the first harmonic terms for the $\mathbf{u}_3$ equation in Equation 3.16

$$(\partial_t - L_0)\mathbf{u}_3^{\pm 1} = K_\pm e^{\pm i\omega_0 t} \tag{3.24}$$

where $K_\pm$ are the coefficients for the ± 1 harmonic terms in Equation 3.23. The $\partial_\tau \mathbf{u}_3^{\pm 1}$ term gives $\pm i\omega_0$, since $\mathbf{u}_3^{\pm 1}$ only contain the first harmonic terms. Now we have

$$(i\omega_0 - L_0)\mathbf{u}_3^{\pm 1} = K_\pm e^{\pm i\omega_0 t} \tag{3.25}$$

From this equation, we cannot solve for the coefficients $K_\pm$ by taking the inverse matrix of $(i\omega_0 - L_0)$, since $i\omega_0$ is the eigenvalue of L_0. Let $\mathbf{u}_3^{\pm 1} = b_\nu^{\pm 1} e^{\pm i\omega_0 t}$, so we could see the explicit dependency on t. We left multiplying by the left eigenvectors $\mathbf{v}^*, \overline{\mathbf{v}}^*$ and get

$$\begin{aligned} \mathbf{v}^*(\partial_t - L_0)\mathbf{u}_3^1 = \mathbf{v}^*(\partial_t - L_0)b_\nu^1 e^{i\omega_0 t} = \mathbf{v}^*(i\omega_0 - i\omega_0)b_\nu^1 e^{i\omega_0 t} = 0 \\ \overline{\mathbf{v}}^*(\partial_t - L_0)\mathbf{u}_3^{-1} = \overline{\mathbf{v}}^*(\partial_t - L_0)b_\nu^{-1} e^{-i\omega_0 t} = \overline{\mathbf{v}}^*(-i\omega_0 - (-i\omega_0))b_\nu^{-1} e^{-i\omega_0 t} = 0 \end{aligned} \tag{3.26}$$

This is called the *solvability condition*, which requires the projection of the first harmonics onto the left eigenvectors to vanish identically. Applying the solvability condition to the corresponding term in Equation 3.23 gives

$$\begin{aligned} 0 = \mathbf{v}^* \left\{ W L_1 \mathbf{v} + |W|^2 W[2M_0(\mathbf{v}A_0 + \overline{\mathbf{v}}A_+) + 3N_0 \mathbf{v}\mathbf{v}\overline{\mathbf{v}}] - \partial_\tau W \mathbf{v} \right\} \quad \Rightarrow \\ \partial_\tau W \mathbf{v}^*\mathbf{v} = W\mathbf{v}^* L_1 \mathbf{v} + |W|^2 W[2\mathbf{v}^* M_0(\mathbf{v}A_0 + \overline{\mathbf{v}}A_+) + 3\mathbf{v}^* N_0 \mathbf{v}\mathbf{v}\overline{\mathbf{v}}] \end{aligned} \tag{3.27}$$

Using the normalization $\mathbf{v}^*\mathbf{v} = 1$ and the identity $\mathbf{v}^* L_1 \mathbf{v} = \lambda_1$, the above equation yields

$$\begin{aligned} &\partial_\tau W = \lambda_1 W - g|W|^2 W, \\ &g = g' + g'' = -2\mathbf{v}^* M_0(\mathbf{v}A_0 + \overline{\mathbf{v}}A_+) - 3\mathbf{v}^* N_0 \mathbf{v}\mathbf{v}\overline{\mathbf{v}}, \quad g' > 0 \end{aligned} \tag{3.28}$$

Notice that W only has τ dependency. So $\varepsilon^2 \partial_\tau = d/dt$

$$\begin{aligned} \Rightarrow \quad \frac{dW}{dt} = \varepsilon^2(\lambda_1 W - g|W|^2 W) \\ \lambda_1 = \sigma_1 + i\omega_1 \ (Eq.3.12) \end{aligned} \tag{3.29}$$

Equation 3.29 is the famous Stuart-Landau equation [22]. The complex amplitude W contains the information of the non-linearity of the system we are analyzing. W has the form of $W = Re^{i\Theta}$, where R is the real-value amplitude, and Θ is the phase. Now Equation 3.29 yields

$$\begin{aligned} \frac{dR}{dt} = \varepsilon^2(\sigma_1 R - g' R^3) \\ \frac{d\Theta}{dt} = \varepsilon^2(\omega_1 - g'' R^2) \end{aligned} \tag{3.30}$$

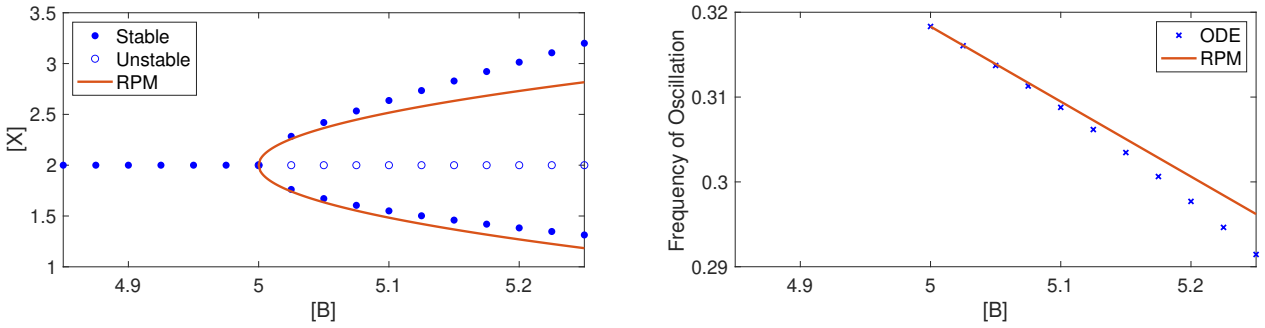

(a) (b)

Figure 3-1: Bifurcation diagrams of (a) concentration of X and (b) frequency of oscillations in the Brusselator model poised near a supercritical Hopf bifurcation. The concentration of A is 2, and bifurcation occurs at $[B] = [A]^2 + 1 = 5$. (a) The central branch is the fixed point, which is stable to the left of criticality (closed circles) and unstable to the right (open circles). The upper and lower branches are the maximum and minimum values of X limit cycle oscillations, calculated numerically (closed blue circles) and using RPM parameters (orange line). (b) The limit cycle frequency is calculated numerically (blue cross marks) and using RPM parameters (orange line).

In long time limit, the complex amplitude W can be portrayed as oscillation with amplitude and frequency

$$\begin{aligned} R_s &= \sqrt{\sigma_1/g'} \\ \omega_s &= \omega_1 - g'' R_s^2 \end{aligned} \tag{3.31}$$

The approximation of $\mathbf{x}$ using the asymptotic solution of Stuart-Landau equation is

$$\mathbf{x} = \mathbf{x}_0 + \varepsilon R_s \left\{ \mathbf{v} e^{i(\omega_0 + \varepsilon^2 \omega_s)t} + \overline{\mathbf{v}} e^{-i(\omega_0 + \varepsilon^2 \omega_s)t} \right\} \tag{3.32}$$

Based on Equation 3.32, for $\mu \approx 0^+$, the amplitude of oscillation is proportional to $\varepsilon = \sqrt{\mu}$, and the frequency of oscillation is proportional to $\varepsilon^2 = \mu$, which agrees with the characteristics of a Hopf bifurcation.

3.2 Example: the Brusselator

We apply the *Reductive Perturbation Method* on the Brusselator model, letting the concentration of A be 2, and the k values be 1. The bifurcation parameter used here is $[B]$, to be consistent with our previous analysis on the Brusselator in this paper. We obtain the bifurcation diagrams for the concentration of X and the frequency of limit cycle oscillation with various $[B]$ values around criticality ($[B] = [A]^2 + 1 = 5$), shown in Figure 3-1. From the two bifurcation diagrams, we see that the RPM approximation of the limit cycle oscillation is accurate, especially when the value of $[B]$ is close to the critical value. The Stuart-Landau parameter values for the Brusselator are shown in Table 3.1. Notice that the ω_0 value, which is the imaginary part of the eigenvalue with zero real part at criticality, indeed agrees with the calculation in Equation 2.20.

Value of $k_1 - k_4$	1
Value of $[A]$	2
Critical value of $[B]$	5
λ_1	$0.5000+2.2328\times10^{-11}$i
ω_0	2.0000
g	0.7500+0.8333i
R_s	1.8257
ω_s	-2.7778
Right Eigenvector (colume)	$\begin{pmatrix} 1.0000+0.0000i \\ -1.0000+0.5000i \end{pmatrix}$
Left Eigenvector (row)	$\begin{pmatrix} 0.5000-1.0000i \\ 0.0000-1.0000i \end{pmatrix}$

Table 3.1: List of Stuart-Landau parameters and eigenvectors of the Brusselator calculated using MATLAB. The bifurcation parameter is the concentration of B.

3.3 RPM Analysis on L2005a Model

The calculation for Stuart-Landau parameters for the circadian rhythms models are implemented in MATLAB. The description of the L2005a system is in Equations 1.1-1.7, and we use the *LHY* transcription rate as bifurcation parameter in this section. Same as in Chapter 2, the transcription rate is normalized by its biological value such that $n_1 = 7.5038\,\text{nM/h}$ corresponds to $\mu = 1$ in the figures and table in this section [23].

For this specific system and bifurcation parameter choice, the behavior of the system is the same under perpetual illumination and perpetual darkness. This is mainly because the light-sensitive protein P_n is uncoupled from other chemical species in the system, as shown in Equations 1.1-1.7. Thus, in this section,

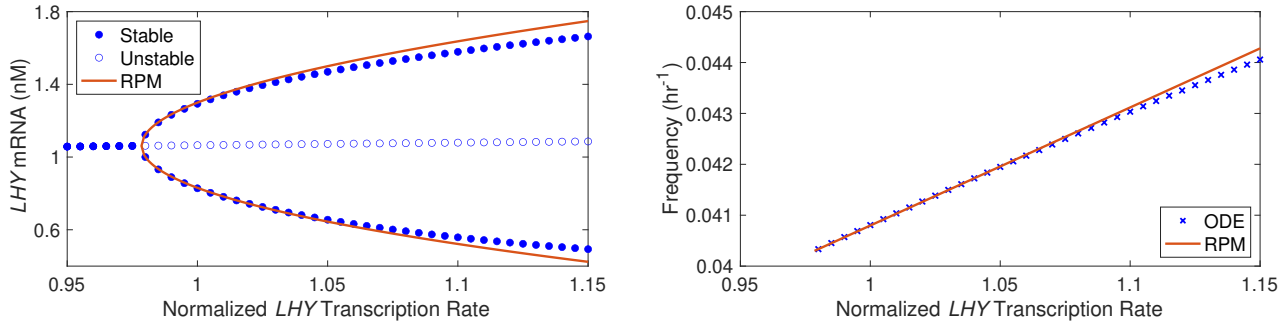

(a) (b)

Figure 3-2: Bifurcation diagrams of (a) concentration of *LHY* mRNA and (b) frequency of circadian oscillations in L2005a model poised near a supercritical Hopf bifurcation under perpetual darkness. The transcription rate of *LHY* is normalized such that the estimated biological value is 1; the bifurcation occurs at 0.9785. (a) The central branch is the fixed point, which is stable to the left of criticality (closed circles) and unstable to the right (open circles). The upper and lower branches are the maximum and minimum values of *LHY* mRNA limit cycle oscillations, calculated numerically (closed blue circles) and using RPM parameters (orange line). (b) The limit cycle frequency is calculated numerically (blue cross marks) and using RPM parameters (orange line).

we show the figures and Stuart-Landau parameters for the light-off case only.

In Figure 3-2a, we compare the bifurcation diagrams for the chemical concentration of *LHY* mRNA calculated using RPM to the numerical solution of the differential equations solved by MATLAB ODE15s solver [21]. In Figure 3-2b, we compare the frequency obtained by RPM and ODE solver. At the biological value of the *LHY* transcription rate (normalized transcription rate = 1 in the figures), the amplitude and the frequency obtained by the two methods agree with each other within 0.86% and 0.45%, respectively. The Stuart-Landau parameters are shown in Table 3.2.

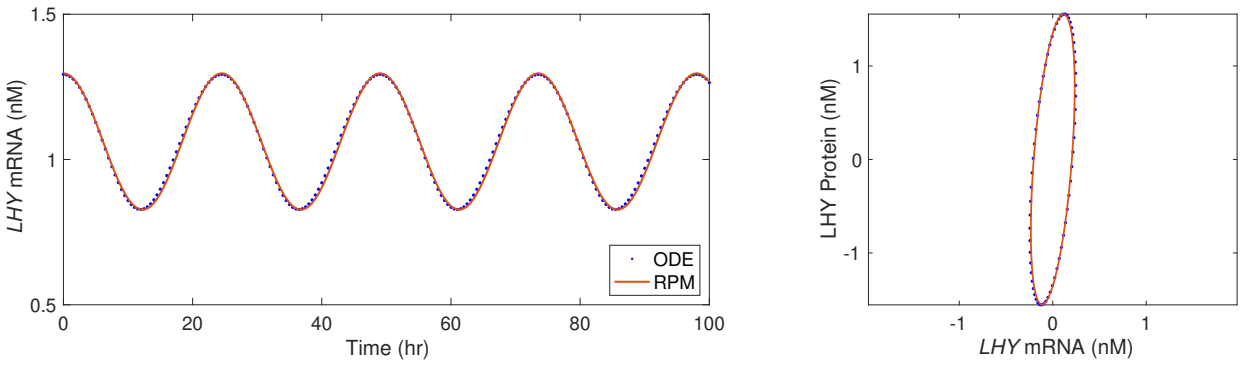

(a) (b)

Figure 3-3: (a) Time series and (b) phase space plot are calculated numerically (ODE) and perturbatively (RPM) for the Locke 2005a model situated near a supercritical Hopf bifurcation under perpetual darkness.

3.4 Discussion

As shown in the comparison figures of the RPM analysis with the numerical solutions, the RPM captures the dynamical behavior of the supercritical system well, as long as the system is sufficiently close to criticality. Usefully, the *Reductive Perturbation Method* collapses the many-dimensional parameter space (29 parameters for L2005a) into the four numbers needed to specify (σ_1, ω_1, g' and g''). This parameter reduction significantly reduces the degrees of freedom when estimating the biological values for the parameters in the circadian rhythms, which may help to overcome the parameter explosion problem described in Section 1.2.

Θ	0 (light-off)
Critical μ	0.9785
Critical biological value	7.3426
λ_1	0.0092+0.0232i
ω_0	0.2532
g	0.1053+0.0389i
R_s	0.7996
ω_s	0.1458
Right Eigenvector (colume)	$\begin{pmatrix} 1.0000 + 0.0000i \\ 3.2616 - 5.7656i \\ 0.4583 - 1.4372i \\ 0.0395 + 0.3512i \\ 11.7250 + 2.2319i \\ 0.6762 + 0.1055i \\ 0.0000 + 0.0000i \end{pmatrix}$
Left Eigenvector (row)	$\begin{pmatrix} 0.0460 + 0.0453i \\ 0.0287 + 0.0387i \\ -0.0006 + 0.0718i \\ 0.2823 - 0.3927i \\ 0.0274 - 0.0160i \\ 0.0408 - 0.0024i \\ 0.1164 + 0.0887i \end{pmatrix}$

Table 3.2: List of Stuart-Landau parameters and eigenvectors of Locke 2005a model under perpetual darkness calculated using MATLAB. The bifurcation parameter is the LHY transcription rate normalized by its biological value ($\mu = 1$ corresponds to the estimated biological value, $n_1 = 7.5038$ nM/h). The second row of the table gives corresponding critical biological values for reference.

Chapter 4

Universality in Kinetic Models

Ten of the eleven models we study possess Hopf bifurcations. However, we found the parameter values that lead to bifurcations are different in different models. Therefore, to compare the behaviors of the ten models, we use the asymptotic variables derived from the *Reductive Perturbation Method* to define dimensionless amplitude and frequency. Then we use the new definition of amplitude and frequency to collapse the ten models onto two universal curves.

4.1 The Degradation Rates

For open systems like the Brusselator and the circadian rhythms models, the dynamics of the system is closely related to the chemical exchange between the system and its environment. One factor that controls such exchange is the degradation of chemicals: holding all the other reaction rates constant, the larger the degradation rates are, the faster the chemicals leave the system, leaving less chemicals in the system to accommodate the reactions. Literature suggests that the circadian rhythms of *Arabidopsis thaliana* are sensitive to the change in degradation rates [24]. Among the *Arabidopsis thaliana* circadian rhythms models we analyze, many employ Michaelis-Menten kinetics for the degradation rates of mRNA and proteins like in L2005a; a few models use linear degradation terms with constant degradation rates. Experimentally, we suppose the degradation rates can be used as a critical control parameter for circadian rhythms networks. Thus, we confined ourselves to search for bifurcation parameters within the chemical degradation rates. We define the normalized, dimensionless degradation rate

$$\mu = \frac{m_c - m}{m_c} \tag{4.1}$$

as the bifurcation parameter (m_c is the critical value of m), so that criticality is at $\mu = 0$. Positive μ values put the system supercritical, where the system undergoes sustained oscillation.

4.2 Data Collapse

To compare the ten models with different rate constants and variables, we want to define new variables that are dimensionless and of universal forms. In the previous chapter, we showed that the limit cycle

oscillation of the circadian rhythms models can be approximated into a universal form with the Stuart-Landau parameters.

At criticality ($\mu = 0$), the system exhibits zero amplitude oscillations about the fixed point. From Equation 3.32,

$$\mathbf{x} = \mathbf{x}_0 + \sqrt{\mu} R_s \left\{ \mathbf{v} e^{i(\omega_0 + \mu\omega_s)t} + \overline{\mathbf{v}} e^{-i(\omega_0 + \mu\omega_s)t} \right\}$$

we can see that the amplitude of oscillation for $\mu \approx 0^+$ is proportional to $\sqrt{\mu}$, and the frequency of oscillation is proportional to μ. The eigenvectors $\mathbf{v}$ and $\overline{\mathbf{v}}$ may be scaled by any constants and remain eigenvectors. If they are scaled by the entry corresponding to the concentration of one of the chemical species, then the amplitude of that chemical species limit cycle oscillation will be $2\sqrt{\mu}R_s$. The chemical species that we use for scaling is arbitrary, so we normalize the eigenvector with respect to its largest entry, which sets the upper bound of the oscillatory amplitude to be $R = 2\sqrt{\mu}R_s$, and frequency of oscillation to be $\omega = \omega_0 + \mu\omega_s$. With these definitions of the amplitude and frequency, we rearrange the terms and obtain the following two parameter-free variables: the "amplitude" $\sqrt{\mu}$ and the "frequency" μ.

$$\frac{R}{2R_s} = \sqrt{\mu}, \qquad \frac{\omega - \omega_0}{\omega_s} = \mu \tag{4.2}$$

4.3 Universal Curves

In Figure 4-1, we show the universal curves, $\sqrt{\mu}$ and μ, and the amplitude and frequency of the oscillations for the ten circadian rhythms models of *Arabidopsis thaliana*. For each model, we calculate the values of R_s and ω_s using the kinetic parameters of the system, and measure the amplitudes and frequencies separately using MATLAB ODE solvers. The measured amplitudes and frequencies are scaled by R_s and ω_s according to Equation 4.2. The scaled amplitudes and frequencies are plotted in log scale, so that the near bifurcation region (for small μ) is amplified. The data points are within 10% from the universal curves. For many models, there are more than one degradation rates that lead to a Hopf bifurcation. For illustrative purposes, we show the results generated using the bifurcation parameter with the largest μ value when the data of either scaled amplitude or frequency diverges from the universal curves by more than 10%. In Appendix B, we show the separate asymptotic amplitude and frequency plots for each model; bifurcation diagrams, time series and phase diagrams similar to Figures 3-2 and 3-3 for each model; and tables of Stuart-Landau parameters and eigenvector entries similar to Table 3.2 for all ten models.

From these universal curves, we see that although the ten models were developed with very different genetic architectures and have completely different sets of parameters, they all exhibit the same dynamical features in the limit cycle oscillations near a Hopf bifurcation. This suggests potential ways to improve the modeling effort, as well as methods for experimentally determining the dynamical properties of the circadian rhythms network. We shall discuss these methods in more detail in the Discussion and Conclusion Chapter (Chapter 6).

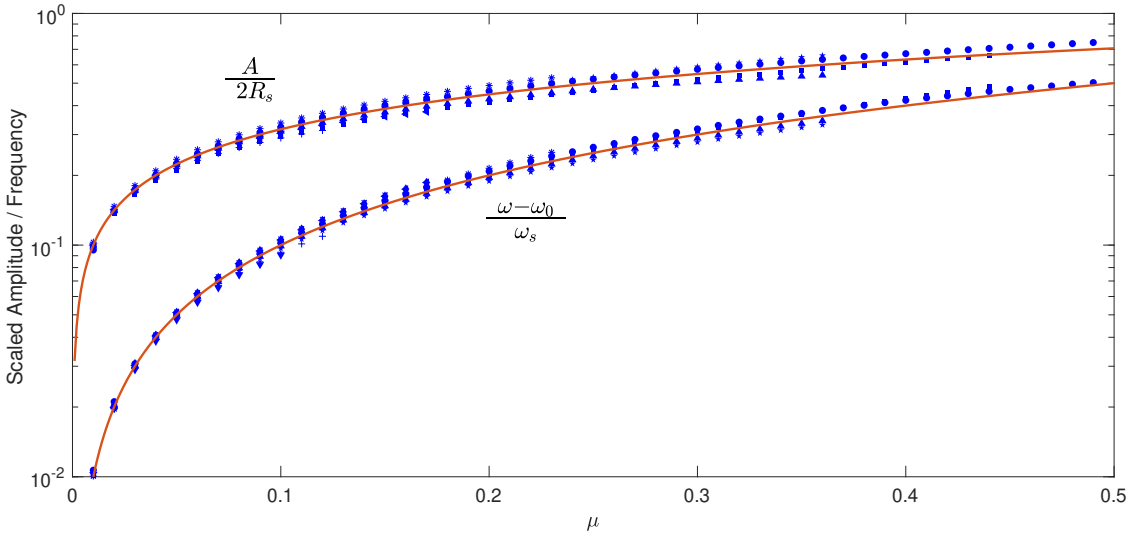

(a) $\Theta = 1$

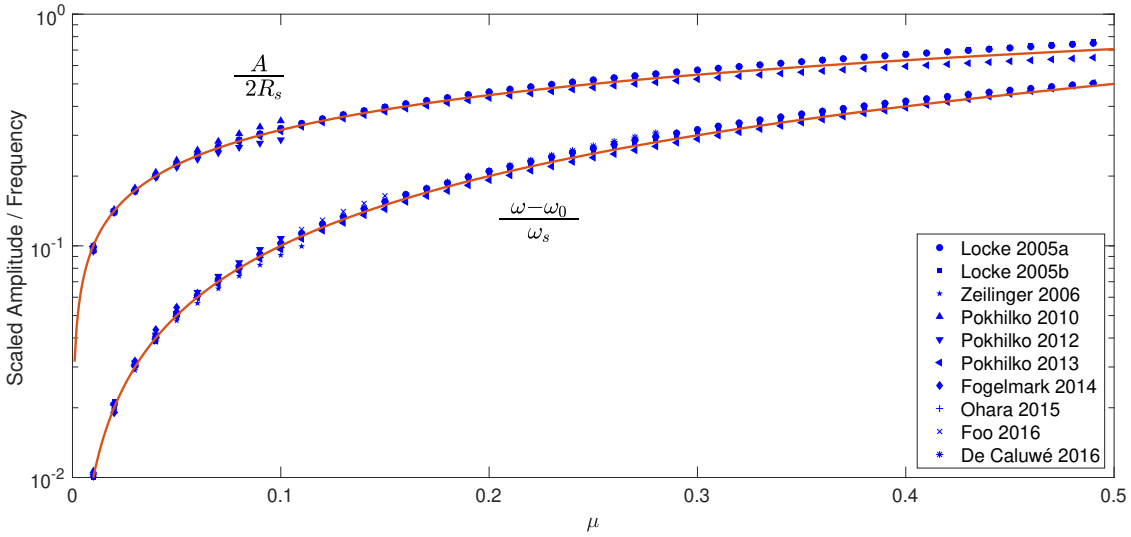

(b) $\Theta = 0$

Figure 4-1: Amplitude (upper) and frequency (lower) of limit cycle oscillations under (a) perpetual illumination, and (b) perpetual darkness for ten models of *Arabidopsis thaliana* circadian rhythms are collapsed onto universal functions of the bifurcation parameter μ. The limit cycle amplitude and frequency are calculated numerically with ODE solvers and scaled according to the Stuart-Landau equation (Equation 4.2). Data for each model is shown up to the value of μ that the data value diverges from one of the universal curves by 10%.

Chapter 5

Stochastic Simulation Algorithm

In the previous chapters, we discussed the behavior of the circadian rhythms of *Arabidopsis thaliana* from the macroscopic scale, by studying the changes in chemical concentrations. Such a purely deterministic approach works well as long as the system is sufficiently large that the chemical concentrations can be treated as continua. However, the chemical reactions occur in a much smaller system: a single plant cell, where some of the key chemicals can be present with molecule numbers as small as a few hundred. Therefore, in the present chapter, we show a stochastic approach that takes the fluctuations in molecular population levels due to each reaction into account.

5.1 Computational Method

The following derivation is adapted from the paper "Exact Stochastic Simulation of Coupled Chemical Reactions" by D.T. Gillespie [14]. We consider a small system where the changes in molecule numbers due to chemical reactions are sufficient to appreciably change the state of the system, and assume that the system is continuously well-mixed and that there is only one reaction launched at any given time. The Gillespie's method uses two values to capture the microscopic behavior of the system: τ, the time step between the end of the previous reaction and the completion of the following reaction; and ξ, the index of the reaction that occurs. We randomly draw two numbers r_1 and r_2 uniformly between 0 and 1 to generate the two values described above using appropriate probability density functions.

Probability of a Reaction Occurring

Consider a chemical reactions system with N species whose molecule numbers are labeled as x_i ($i = 1, 2, \cdots, N$) and M chemical reactions labeled as R_j ($j = 1, 2, \cdots, M$). For a chemical reaction R_ξ with reactants a and b, its reaction rate $c_\xi dt$ is defined as the average probability that a particular a-b molecule pair will react according to R_ξ in the next infinitesimal time interval dt. This definition of c_ξ is called the *fundamental hypothesis* of the stochastic formulation of chemical kinetics, which holds true for a well-mixed system. The rate c_ξ, a volume-dependent parameter, is related to but not to be confused with the reaction rate k in the continuous case. The probability of reaction R_ξ occurring at time t is related to the number of distinct possible a-b pairs, h_ξ. Using elementary combinatorics, if the reactants are of different species, then $h_\xi = x_a x_b$; if $a = b$, then $h_\xi = x_a(x_a - 1)/2$. Now, for each reaction R_ξ, we may define $a_\xi dt \equiv h_\xi c_\xi dt =$

Probability of R_ξ occurring in time interval $(t, t+dt)$ given the state of the system at time t. Moreover, let a_0 be the sum of all a_ξ.

Calculating τ and ξ from the Reaction Probability Density Function

The goal of the Gillespie method is to determine a joint probability density function $P(\tau, \xi)$ such that $P(\tau, \xi)d\tau$ is the probability that, given the state of the system at time t, the next reaction in the system will occur between time $(t+\tau)$ and time $(t+\tau+d\tau)$ *and* it will be the reaction R_ξ. To determine $P(\tau, \xi)$, we first express it as

$$P(\tau, \xi) = P_0(\tau) \cdot a_\xi d\tau \tag{5.1}$$

where $P_0(\tau)$ is the probability that given the state of the system at time t, no reaction will occur between time t and time $t+\tau$, and $a_\xi d\tau$ is the probability that the reaction R_ξ will occur in the next time interval $(t+\tau)$ to $(t+\tau+d\tau)$. First, we determine $P_0(\tau)$ by noting that $a_0 d\tau$ is the probability that some reaction will occur in the time interval $d\tau$ and thus $[1 - a_0 d\tau]$ is the probability that no reaction will occur in time interval $d\tau$. Meanwhile, the probability $P_0(\tau + d\tau)$ that no reaction occurs between time t and time $t+\tau+d\tau$ is the product of the probability that no reaction occurs between time t and time $t+\tau$ and the probability that no reaction occurs between time $t+\tau$ and time $t+\tau+d\tau$,

$$\begin{aligned} & P_0(\tau + d\tau) = P_0(\tau)\,[1 - a_0 d\tau] \\ \Rightarrow \quad & \frac{P_0(\tau + d\tau) - P_0(\tau)}{d\tau} = \frac{dP_0(\tau)}{d\tau} = -a_0 P_0(\tau) \\ \Rightarrow \quad & P_0(\tau) = e^{-a_0 \tau} \end{aligned} \tag{5.2}$$

The probability density function in Equation 5.1 may now be written as

$$P(\tau, \xi) = P_0(\tau) \cdot a_\xi d\tau = a_\xi e^{-a_0 \tau} \tag{5.3}$$

which may be broken into two normalized distributions:

$$P_1(\tau) = a_0 e^{-a_0 \tau}, \quad P_2(\xi) = \frac{a_\xi}{a_0} \qquad \Rightarrow \qquad P_1(\tau) \cdot P_2(\xi) = P(\tau, \xi) \tag{5.4}$$

Now, the time of the next reaction τ, and the next reaction to occur R_ξ, may be determined by drawing random numbers from the distributions $P_1(\tau)$ and $P_2(\xi)$. This is achieved computationally by drawing two random numbers r_1 and r_2 from the uniform distribution on the unit interval $(0, 1)$ and computing

$$\tau = \frac{1}{a_0} \ln\left(\frac{1}{r_1}\right) \qquad \sum_{\nu=1}^{\xi-1} a_\nu < r_2 a_0 \leq \sum_{\nu=1}^{\xi} a_\nu \tag{5.5}$$

Figure 5-1 illustrates the meaning of τ and ξ in pictorial form. As Figure 5-1b shows, the larger a_ξ is, the more probable the reaction will occur.

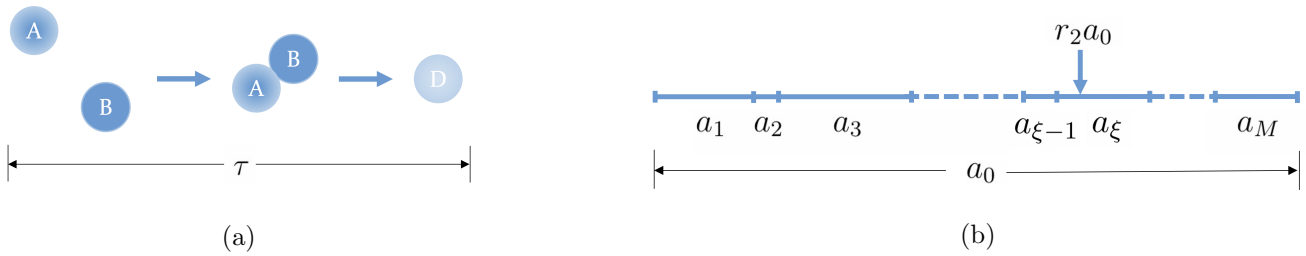

(a) (b)

Figure 5-1: Schematic picture of the meaning of the two parameters, τ and ξ, in the *Stochastic Simulation Algorithm*. (a) τ shows the time between the completion of two consecutive chemical reactions. (b) $a_j dt$ $(j = 1, 2, \cdots, M)$ shows relative probability that the reaction happening at time $t + \tau$ is R_j, and a_0 is the sum of all a_j. The larger a_j is, the more probable a reaction will occur. ξ is the index of the reaction that occurs, determined by the random value r_2.

The Algorithm

The *Stochastic Simulation Algorithm* captures the changes in molecule numbers at each time step τ according to the reaction R_ξ. If the species appears on the reactant side of the chemical reaction, the molecule number decreases by its coefficient; if the species is on the product side, the number of molecule increases by its coefficient.

The algorithm takes the following steps:

1. Initialization: input the M reactions with the reaction constants c_j, and the N chemical species involved with the initial values of molecule numbers x_i. Set the total reaction (simulation) time T. Set time t and reaction counter n to zero.

2. Calculation: generate and store the values of a_j for the M reactions, and calculate the value of $a_0 = \sum a_j$.

3. SSA parameters: generate the two random numbers r_1 and r_2, and calculate the corresponding τ and ξ according to Equation 5.5.

4. System update: Increase t by τ, and update the molecule numbers according to reaction R_ξ. The reaction counter n increases by 1. Then repeat steps 2-4 until $t \geq T$.

5.2 Example: the Brusselator

From the reaction equations introduced in Section 1.3, the SSA parameters for the Brusselator model with volume V are shown in Table 5.1. The changes in molecular numbers according to each reaction are described in the array *Channels*

$$\text{Channels} = \begin{bmatrix} 1 & 1 & -1 & -1 \\ 0 & -1 & 1 & 0 \end{bmatrix} \tag{5.6}$$

Each column of "Channels" corresponds to a reaction. The first row is the molecule number changes of X, and the second row is of Y.

j	Reaction (R_j)	c_j	h_j	$a_j = c_j \cdot h_j$
1	$A \xrightarrow{k_1} X$	sk_1	A	$sk_1 A$
2	$2X + Y \xrightarrow{k_2} 3X$	sk_2	$\frac{1}{2}X \cdot (X-1) \cdot Y$	$\frac{sk_2}{2} X \cdot (X-1) \cdot Y$
3	$B + X \xrightarrow{k_3} Y + D$	sk_3	$B \cdot X$	$sk_3 B \cdot X$
4	$X \xrightarrow{k_4} E$	sk_4	X	$sk_4 X$

Table 5.1: Parameters used in the stochastic simulation for each reaction in the Brusselator. The c values are closely related the the reaction constants k, with a volume scaling factor s. h is the number of distinct molecule groups that could react according to R_j.

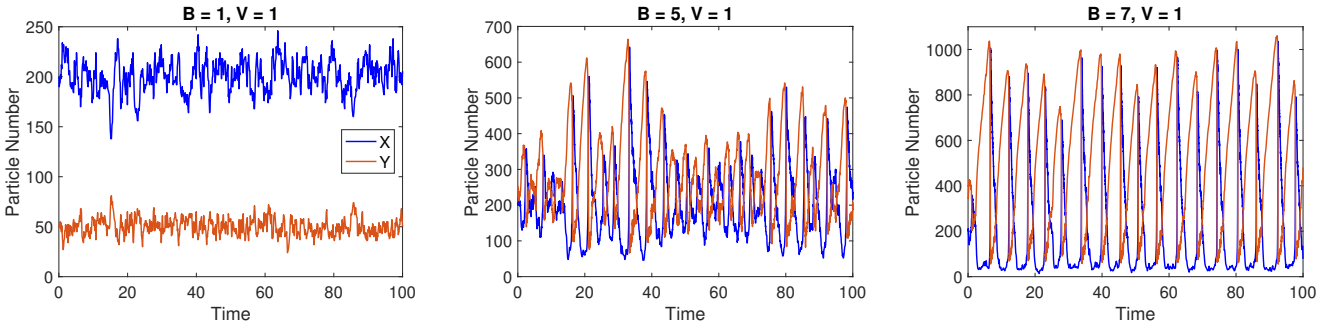

(a) (b) (c)

Figure 5-2: Stochastic simulation time series of the Brusselator with (a) $[B] = 1$ (subcritical in deterministic limit), (b) $[B] = 5$ (criticality in deterministic limit), and (c) $[B] = 7$ (supercritical in deterministic limit). The concentration of A is 2, and the volume of the system is 1 unit.

Figure 5-2 shows the stochastic simulation time series for the Brusselator for both supercritical and subcritical. Though the signals are noisy due to the nature of the stochastic algorithm, we can still see the overall trend of a stable equilibrium for the subcritical case, and sustained oscillations for the supercritical case. Moreover, in Figure 5-3, we take the subcritical case as an example, and show that while keeping all other parameters unchanged, the relative fluctuation diminishes as the volume of the system increases, and the behavior of the signal approaches the deterministic solution as shown in Figure 2-1a.

5.3 SSA Analysis on L2005a Model

To apply the SSA method on the L2005a model, we first need to identify the pseudo reactions in the system. The procedure follows closely with the *Law of Mass Action* introduced in Section 1.3. Using the differential equation for the LHY mRNA under perpetual darkness as an example

$$\frac{d[L_m]}{dt} = \frac{n_1[T_n]}{g_1 + [T_n]} - \frac{m_1[L_m]}{k_1 + [L_m]}$$

The first term of the right-hand side of the ODE can be considered as $\frac{n_1[T_n]}{g_1+[T_n]} = \frac{n_1}{g_1+[T_n]} \cdot [T_n]$. We put T_n on the reactant side, since the *Law of Mass Action* states that the probability of a reaction occurring is proportional to the concentration of reactants. The rest of the fraction ($\frac{n_1}{g_1+[T_n]}$) is considered as the pseudo reaction rate. Since this term is positive, the amount of L_m increases when the reaction occurs. In the

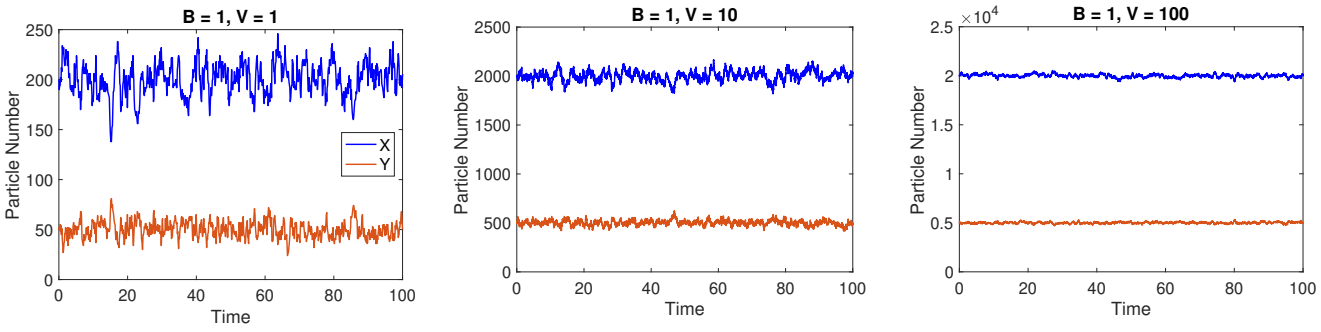

(a) (b) (c)

Figure 5-3: Stochastic simulation time series of the Brusselator with $[B] = 1$ (subcritical), $[A] = 2$. The volume of the system is (a) 1 unit, (b) 10 units, and (c) 100 units. The signal becomes less noisy as the volume increases and approaches the signal for deterministic system.

molecular level, we say the molecule number of L_m will increase by 1, which means L_m is on the product side. What is more, there is not a corresponding term in the T_n differential equation, meaning that the molecule number of T_n does not change through this reaction. So, T_n also shows up on the product side. Therefore, the pseudo reaction translated from the first term in the ODE is $T_n \to L_m + T_n$ with reaction rate $c = \frac{sn_1}{g_1+[T_n]}$ where s is the volumn scaling factor. Similarly, the second term in the ODE gives the pseudo reaction for L_m degradation: $L_m \to X_1$ with $c = \frac{sm_1}{k_1+[L_m]}$. In this reaction, X_1 is a species in the sink of the system.

There are 16 reactions identified from the system of differential equations for L2005a, and each reaction takes one of the following four forms:

$$B \leftrightarrow C \qquad A \to \phi \qquad A \to A + B \qquad \phi \to D \tag{5.7}$$

The capitalized English letters represent chemical species in the system; the term ϕ refers to chemicals outside of the system, and we assume that the system has infinite source and sink. Notice that all of the four forms of reactions has only one chemical species as reactant, so there is no collision between reactant molecules required. Starting from the left, the four types of reactions refer to: 1. transport of proteins across the nucleus membrane; 2. degradation of chemical species; 3. translation from mRNA to protein in the cytoplasm, or activation on the LHY mRNA by the TOC1 protein in the nucleus; and 4. the reactions through which the light sensitive protein P_n is produced. Figure 5-4 is the schematic picture of the 16 reactions. The complete set of pseudo chemical reactions is included in Appendix C.1.

To define the size of the system for the stochastic simulation, we approximate a plant cell to be a sphere with 100 microns in diameter. The typical concentration of protein molecules in cells is about 1 nM/m^3. Using the estimated volume of plant cell, the molecule concentration, and the Avogadro's number ($N_A = 6.02 \times 10^{23}$/M), we estimate that there are about 315 molecules of each of the seven chemical species in the circadian rhythms system. This molecular population value is used as the initial condition for the stochastic simulation. The system size in our simulations uses single plant cell as unit.

In Figure 5-5a, we show the time series result of the *Stochastic Simulation Algorithm* for a single plant cell. Although the signal is very noisy, due to the nature of the stochastic simulation, we can still see

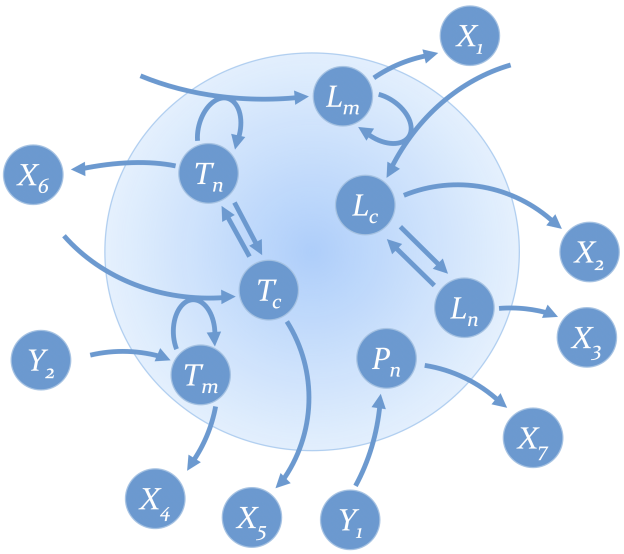

Figure 5-4: The schematic picture of pseudo chemical reactions in L2005a model. The large circle is the plant cell where all the reactions take place in, and the darker small circles labeled with the species names are the seven chemical species that we study. The system is assumed to have infinite source and sink, ϕ (the outside of the large circle, that is, the amounts of species labeled with X_i and Y_i are held constant. Notice that there is no collision required for this set of reactions.

periodic oscillations with period of approximately 24-25 hours. In Figures 5-5b and 5-5c, we show the time series of the stochastic simulation for systems of larger sizes. As the system size increases, the relative size of noise becomes smaller. Comparing the results of the larger systems with the behavior of the deterministic solution as shown in Figure 5-5d, we conclude that the results of *Stochastic Simulation Algorithm* approach the behavior of the deterministic system when the size of the system increases, as expected.

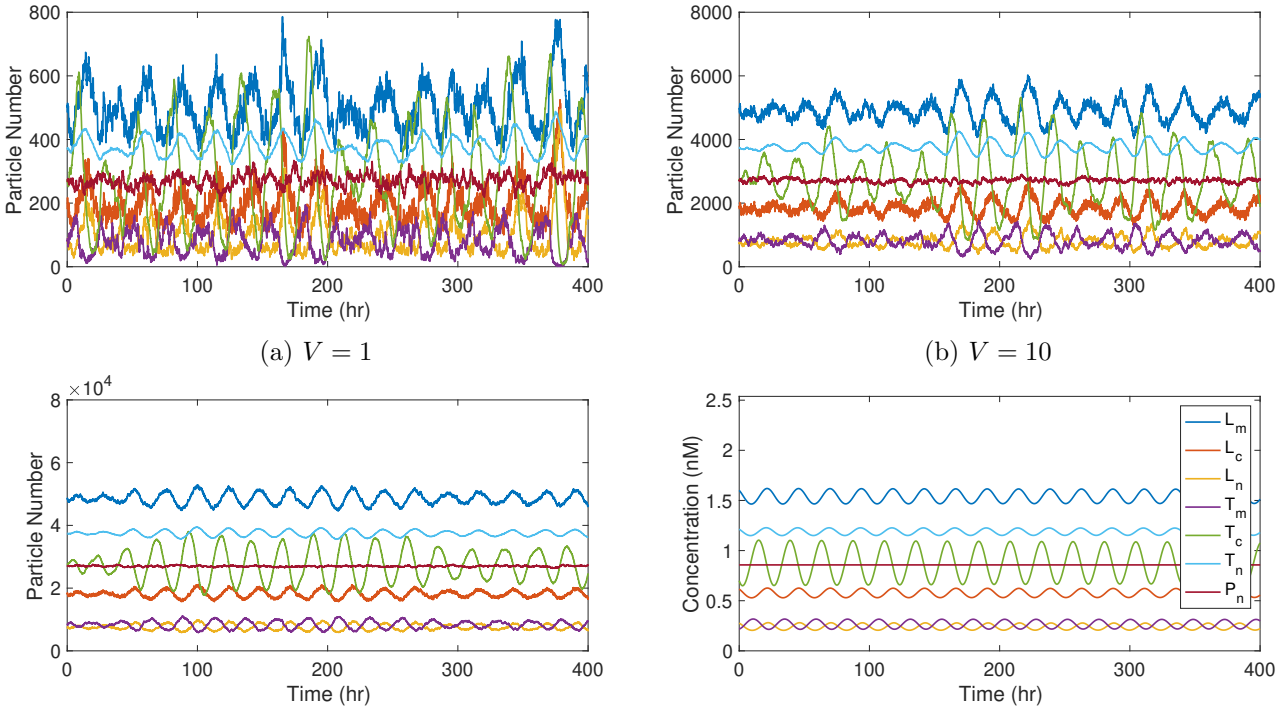

(a) $V = 1$ (b) $V = 10$

(c) $V = 100$ (d) Deterministic

Figure 5-5: Stochastic simulation time series of the Locke 2005a circadian rhythms model with (a) $V = 1$, (b) $V = 10$, and (c) $V = 100$. We also include (d) time series of the system obtained by the MATLAB ODE15s solver. The rate constants besides m_1 take the optimal values determined in the Locke *et al.* 2005a paper. The m_1 value for all four figures is 8.8978 nM/h, which is on the supercritical side of the Hopf bifurcation. The volume of the system uses approximate size of single plant cell as unit.

Chapter 6

Discussion and Conclusion

In this thesis, we analyzed the dynamics of circadian rhythms of *Arabidopsis thaliana* using published models. At the macroscopic scale of the whole plant, we demonstrated that the published models possess supercritical Hopf bifurcations. We used that fact to perform a weakly nonlinear analysis method *Reductive Perturbation Method* valid near the bifurcation point. We further simulated the stochastic dynamics of circadian rhythms at the microscopic single-cell level by interpreting the differential equations as their elementary reactions and employing the *Stochastic Simulation Algorithm*.

In Chapters 3 and 4, we employed the *Reductive Perturbation Method* of Y. Kuramoto to derive a two-dimensional approximation of the chemical oscillations of the models near their bifurcations. We scaled the amplitude and frequency of oscillations with the asymptotic solution of the Stuart-Landau equation to collapse all models onto two universal curves, and showed that they exhibit the same dynamical behavior near the Hopf bifurcation.

Though we found all the models exhibit the same dynamical behavior near bifurcation, we also discovered that important dynamical features are inconsistent among the models. According to the numerical solutions of the ODE systems using the optimal values of rate constants provided in the original papers, some models are situated on the supercritical side of Hopf bifurcation, while the others are on the subcritical side. When we searched among the degradation rates for potential bifurcation parameters, we found rate constants that lead to a Hopf bifurcation in some models do not lead to a Hopf bifurcation in other models. Another significant difference across the models is the distances from bifurcation, as well as how nonlinear the models are. In the bifurcation diagrams for each model, we measured the percentage differences of the RPM approximations to the numerical solutions. In the Locke *et al.* 2005a model, the RPM approximation of amplitude presented in Section 3.3 matches the numerically solved limit cycle amplitude with less than 0.8% error, while the RPM calculation of limit cycle amplitude of Pokhilko *et al.* 2010 model presented in Appendix B varies from the numerically solved amplitude by 45.02%. These important dynamical features should agree across models, as all ten mathematical models describe the same biological system. A potential reason for these discrepancies is the search-and-check modeling method with large degrees of freedom. It is worth noting that none of these reaction rates are accessible experimentally. Having shown the search-and-check scheme does not produce dynamically reliable results, we suggest our lower dimensional approach is more appropriate.

The *Reductive Perturbation Method* suggests improvements of modeling work that address the difficul-

ties mentioned above. Experimentally, we suggest a possible method to test out whether the biological system is supercritical or subcritical using the resonance frequency of the system. In this experiment, a resonance curve would be measured with sinusoidal light sources of a range of frequencies near the natural frequency of the circadian rhythms system. The side of Hopf bifurcation that the system is located can be found through the dependence of the amplitude of oscillation on the driving frequency [25]. Computationally, the *Reductive Perturbation Method* simplifies the higher-dimensional models into the two-dimensional eigenspace, and describes the models using only the four Stuart-Landau parameters $(\sigma_1, \omega_1, g', g'')$ instead of the large number of rate constants.

While circadian rhythms can be successfully modeled with differential equations, physically the chemical reactions of the circadian rhythms are occurring at the single-cell level where there are too few molecules to satisfy a continuum description. Thus in Chapter 5, we used the *Stochastic Simulation Algorithm* to show that at the cellular level, the system still exhibits circadian oscillations in molecule numbers. We showed further that in the limit that the system size goes to infinity, the stochastic simulation result matches the deterministic solution. More simulation work can be done using *Stochastic Simulation Algorithm* to produce similar plots as the bifurcation diagrams for the deterministic systems, although the definition of measured amplitude and frequency need to be redefined because the stochastic nature of the signals exhibit random fluctuations comparable to the oscillation amplitude. These plots would show if the stochastic system obeys similar relationships between the amplitude and frequency of oscillation and the bifurcation parameter.

Lastly, recent experiments have shown that circadian oscillations in the cyanobacterium *Synechoccus elongatus*, one of Earth's most ancient and simplest form of life, exhibit a supercritical Hopf bifurcation when the temperature is varied [26]. Physicists studying the biological systems have aimed to find physical organizing principles in living systems. Hopf bifurcations appear to occur in a number of biological oscillators such as the hair cells of the cochlea in the ears of humans [25, 27] and frogs [28], and the glycolytic oscillations in yeast *Saccharomyces cerevisiae* [29]. This suggests that Hopf bifurcation may be a property favored during the evolutionary development of biological systems. By studying Hopf bifurcations in circadian rhythms, we contribute to the goal of uncovering physical organizing principles in living organisms.

Bibliography

[1] Andrew J Millar. "The intracellular dynamics of circadian clocks reach for the light of ecology and evolution". In: *Annual review of plant biology* 67 (2016), pp. 595–618.

[2] James CW Locke, Andrew J Millar, and Matthew S Turner. "Modelling genetic networks with noisy and varied experimental data: the circadian clock in Arabidopsis thaliana". In: *Journal of theoretical biology* 234.3 (2005), pp. 383–393.

[3] James CW Locke et al. "Extension of a genetic network model by iterative experimentation and mathematical analysis". In: *Molecular systems biology* 1.1 (2005), p. 0013.

[4] James CW Locke et al. "Experimental validation of a predicted feedback loop in the multi-oscillator clock of Arabidopsis thaliana". In: *Molecular systems biology* 2.1 (2006), p. 59.

[5] Melanie N Zeilinger et al. "A novel computational model of the circadian clock in Arabidopsis that incorporates PRR7 and PRR9". In: *Molecular Systems Biology* 2.1 (2006), p. 58.

[6] Alexandra Pokhilko et al. "Data assimilation constrains new connections and components in a complex, eukaryotic circadian clock model". In: *Molecular systems biology* 6.1 (2010), p. 416.

[7] Alexandra Pokhilko et al. "The clock gene circuit in Arabidopsis includes a repressilator with additional feedback loops". In: *Molecular systems biology* 8.1 (2012), p. 574.

[8] Alexandra Pokhilko, Paloma Mas, and Andrew J Millar. "Modelling the widespread effects of TOC1 signalling on the plant circadian clock and its outputs". In: *BMC systems biology* 7.1 (2013), p. 23.

[9] Karl Fogelmark and Carl Troein. "Rethinking transcriptional activation in the Arabidopsis circadian clock". In: *PLoS computational biology* 10.7 (2014), e1003705.

[10] Takayuki Ohara, Hirokazu Fukuda, and Isao T Tokuda. "An extended mathematical model for reproducing the phase response of Arabidopsis thaliana under various light conditions". In: *Journal of theoretical biology* 382 (2015), pp. 337–344.

[11] Mathias Foo, David E Somers, and Pan-Jun Kim. "Kernel architecture of the genetic circuitry of the Arabidopsis circadian system". In: *PLoS computational biology* 12.2 (2016), e1004748.

[12] Joëlle De Caluwé et al. "A compact model for the complex plant circadian clock". In: *Frontiers in plant science* 7 (2016), p. 74.

[13] Yoshiki Kuramoto. *Chemical oscillations, waves, and turbulence*. Springer-Verlag, Berlin, Heidelberg, 1984.

[14] Daniel T Gillespie. "Exact stochastic simulation of coupled chemical reactions". In: *The journal of physical chemistry* 81.25 (1977), pp. 2340–2361.

[15] John J Tyson. "Some further studies of nonlinear oscillations in chemical systems". In: *The Journal of Chemical Physics* 58.9 (1973), pp. 3919–3930.

[16] J.D. Murray. *Mathematical Biology*. Biomathematics. Springer Berlin Heidelberg, 2013. ISBN: 9783662085394. URL: https://books.google.com/books?id=K3LmCAAAQBAJ.

[17] Leland H Hartwell and Michael B Kastan. "Cell cycle control and cancer". In: *Science* 266.5192 (1994), pp. 1821–1828.

[18] DAVID Paydarfar and FREDERIC L Eldridge. "Phase resetting and dysrhythmic responses of the respiratory oscillator". In: *American Journal of Physiology-Regulatory, Integrative and Comparative Physiology* 252.1 (1987), R55–R62.

[19] Brian D Hassard, Nicholas D Kazarinoff, and Y-H Wan. *Theory and applications of Hopf bifurcation*. Vol. 41. CUP Archive, 1981.

[20] Caitlin McCann. "Bifurcation Analysis of Non-linear Differential Equations". In: ().

[21] Lawrence F Shampine and Mark W Reichelt. "The matlab ode suite". In: *SIAM journal on scientific computing* 18.1 (1997), pp. 1–22.

[22] John Trevor Stuart. "On the non-linear mechanics of hydrodynamic stability". In: *Journal of Fluid Mechanics* 4.1 (1958), pp. 1–21.

[23] Isao T Tokuda, Ozgur E Akman, and James CW Locke. "Reducing the complexity of mathematical models for the plant circadian clock by distributed delays". In: *Journal of theoretical biology* 463 (2019), pp. 155–166.

[24] Esther Yakir et al. "CIRCADIAN CLOCK ASSOCIATED1 transcript stability and the entrainment of the circadian clock in Arabidopsis". In: *Plant physiology* 145.3 (2007), pp. 925–932.

[25] Vıctor M Eguluz et al. "Essential nonlinearities in hearing". In: *Physical review letters* 84.22 (2000), p. 5232.

[26] Yoriko Murayama et al. "Low temperature nullifies the circadian clock in cyanobacteria through Hopf bifurcation". In: *Proceedings of the National Academy of Sciences* 114.22 (2017), pp. 5641–5646.

[27] AJ Hudspeth, Frank Jülicher, and Pascal Martin. "A critique of the critical cochlea: Hopf—a bifurcation—is better than none". In: *Journal of neurophysiology* 104.3 (2010), pp. 1219–1229.

[28] Mark Ospeck, Vıctor M Eguluz, and Marcelo O Magnasco. "Evidence of a Hopf bifurcation in frog hair cells". In: *Biophysical journal* 80.6 (2001), pp. 2597–2607.

[29] Sune Danø, Preben Graae Sørensen, and Finn Hynne. "Sustained oscillations in living cells". In: *Nature* 402.6759 (1999), pp. 320–322.

Appendix A

Using the MATLAB Code

A.1 Reductive Perturbation Method and Universality of Kinetic Models

The RPM_Code folder contains the Grand_MostDataPoints.m file, and ten folders, one for each model. **Grand_MostDataPoints.m** runs the simulation for all models and uses the bifurcation parameter that gives the most data points on bifurcation diagrams with the set percentage error criteria. Each model folder contains the following files:

1. **Main_[ModelName].m** which includes all major steps for choosing bifurcation parameter and calculating Stuart-Landau parameters.

2. **Simulate_Circadian_[ModelName].m** which includes the steps for simulation using MATLAB ODE solver.

3. **Circadian_[ModelName].mlx** which is the live script function file including all ODEs. The typeset equations and set(s) of parameter values are also included in this file.

4. **Circadian_syms_[ModelName].m** which is the function file including all ODEs. This file is identical to item 3, but all the parameters and variables are symbolic variables using MATLAB Symbolic Toolbox.

5. **Filter.m** which finds all degradation rates that lead to bifurcation. The searching range of bifurcation is between 0 to the optimal value for subcritical models, and between optimal value to 3 times of optimal value for supercritical models. The critical values are also generated through this process.

6. **Solve_cp.m** which solves for critical values of the bifurcation parameters with given range. The function uses binary search.

7. **Generate_values.m** which, for each degradation rate that leads to a bifurcation, calculates Stuart-Landau parameters ω_0 and g, as well as the eigenvalues and eigenvectors of the Jacobian evaluated at criticality.

8. **Calc_sigma_omega.m** which, for each degradation rate that leads to a bifurcation, calculates the values of σ_1 and ω_1.

9. **Calc_lambdas.m** which returns the two eigenvalues with largest real parts. These two eigenvalues should be complex conjugates of each other.

10. **Jacobian.m** which generates the symbolic Jacobian of the system of equations, L.

11. **third_tensor.m** which generates the symbolic third degree tensor of the system of equations, M.

12. **fourth_tensor.m** which generates the symbolic fourth degree tensor of the system of equations, N.

13. **FixedPt.m** which finds the fixed point of the system of equations with given parameter values. The function uses MATLAB fsolve.

14. **Evaluation.m** which substitutes in values for parameter values in a symbolic expressions, e.g. L, M and N.

15. **Evaluation_fp.m** which substitutes in values for variables at fixed point in a symbolic expressions, e.g. L, M and N.

16. **Mult.m** which multiplies a tensor and a vectot together. This function compresses the tensor along the last dimension.

17. **eigen.m** which returns sorted eigenvalues and eigenvectors. The eigenvalues and eigenvectors are sorted with respect to real parts of eigenvalues from small to large.

For the models that are supercritical with biological parameter values in either perpetual illumination or perpetual darkness, the following files are also included:

18. **BifurcationDiagram_TimeSeries_[ModelName].m**
    which generates 4 plots: time series of LHY mRNA; time series of $TOC1$ mRNA; bifurcation diagram of concentration of LHY mRNA to show fixed point and limit cycle; bifurcation diagram of oscillatory frequency which is only plotted for the supercritical side of bifurcation. The bifurcation diagrams convert $\mu = 1$ to be the biological value given in the original paper of bifurcation parameter.

19. **PhaseDiagram_[ModelName].m** which generates 3 plots: phase diagram of LHY protein vs. LHY mRNA; phase diagram of TOC1 protein vs. $TOC1$ mRNA; phase diagram of $TOC1$ mRNA vs. LHY mRNA. The phase diagrams reflect phase relationship at $\mu = 1$, the biological value given in the original paper of bifurcation parameter.

20. **atan_0to2pi.m** which calculates arctangent value of the input, and shifts the range to 0 to 2π.

These can only be run after obtaining information of bifurcation for the model from above steps. All plots include data points or curves from both RPM method and ODE solutions for comparison.

A.2 Stochastic Simulation Algorithm

The The SSA_Code folder contains the **Simulate_Circadian.m** file, which is the main file for the *Stochastic Simulation Algorithm* on the Locke *et al.* 2005a circadian rhythms model. The following files are included in the folder:

1. **Circadian.m** which includes differential equations of the circadian rhythms model.
2. **Solve_Circadian.m** which solves the system deterministically using the ODE15s solver, and finds initial conditions for the simulation.
3. **Scale.m** which scales all constants / initial conditions in terms of molecule numbers with respect to the volume of the system.
4. **Calculat_a.m** which calculates the values of a_i's.
5. **Randomize.m** which generates random values to determine the time step (τ) and the index of reaction taking place (ξ).
6. **rpdPlot.m** which trims off empty entries at the end of arrays and plots every nth data point.
7. **rms_vs_mu** which plots $rmsd$ vs. m_1 around bifurcation point ($m_1 = 8.9978; m_4 = 1.6859$). This function is not used in the main file.

Appendix B

Supplementary Figures and Tables of Chapter 4

In figures B-2-B-12, for all the models we studied whose reported optimal parameters give a supercritical system, we show: 1) bifurcation diagrams for limit cycle amplitude and frequency of *LHY* mRNA, 2) time series for *LHY* mRNA and *TOC1* mRNA limit cycle oscillations, and 3) phase space plots for LHY and TOC1 protein oscillations and *LHY* and *TOC1* mRNA oscillations. Each figure compares the numerical results of the full system of differential equations to the result of the *Reductive Perturbation Method*[13].

In figures B-13 and B-14, we collapse the limit cycle amplitude and frequency of all the models using their respective natural scales. The data is identical to that plotted in Figure 4-1 of the main text , but plotted separately for each model.

In tables B.1 and B.2 we show: 1) the kinetic parameter used as the Hopf bifurcation parameter (BP) to produce the data in figure 3 of the main text and figures B-1-B-14, 2) the chemical species with the largest modulus used to scale the eigenvectors of the Jacobian matrix at the bifurcation point used to calculate the natural scales, 3) the optimal value of the BP given in the original paper, 4) the critical value of the BP where the Hopf bifurcation occurs, 5) the frequency of zero amplitude oscillations at the bifurcation point, 6) the value of the complex number g in the Stuart-Landau equation, 7) the value of the first order Taylor expansion term, λ_1, of the eigenvalue of the Jacobian matrix near the bifurcation point.

In tables B.3-B.8, we show the several elements of the eigenvectors of the Jacobian matrix at the bifurcation point, normalized by the largest modulus entry, that correspond to LHY and TOC1 protein and *LHY* and *TOC1* mRNA concentrations.

B.1 Bifurcation Diagrams, Time Series, and Phase Diagrams for Supercritical Models under Perpetual Illumination

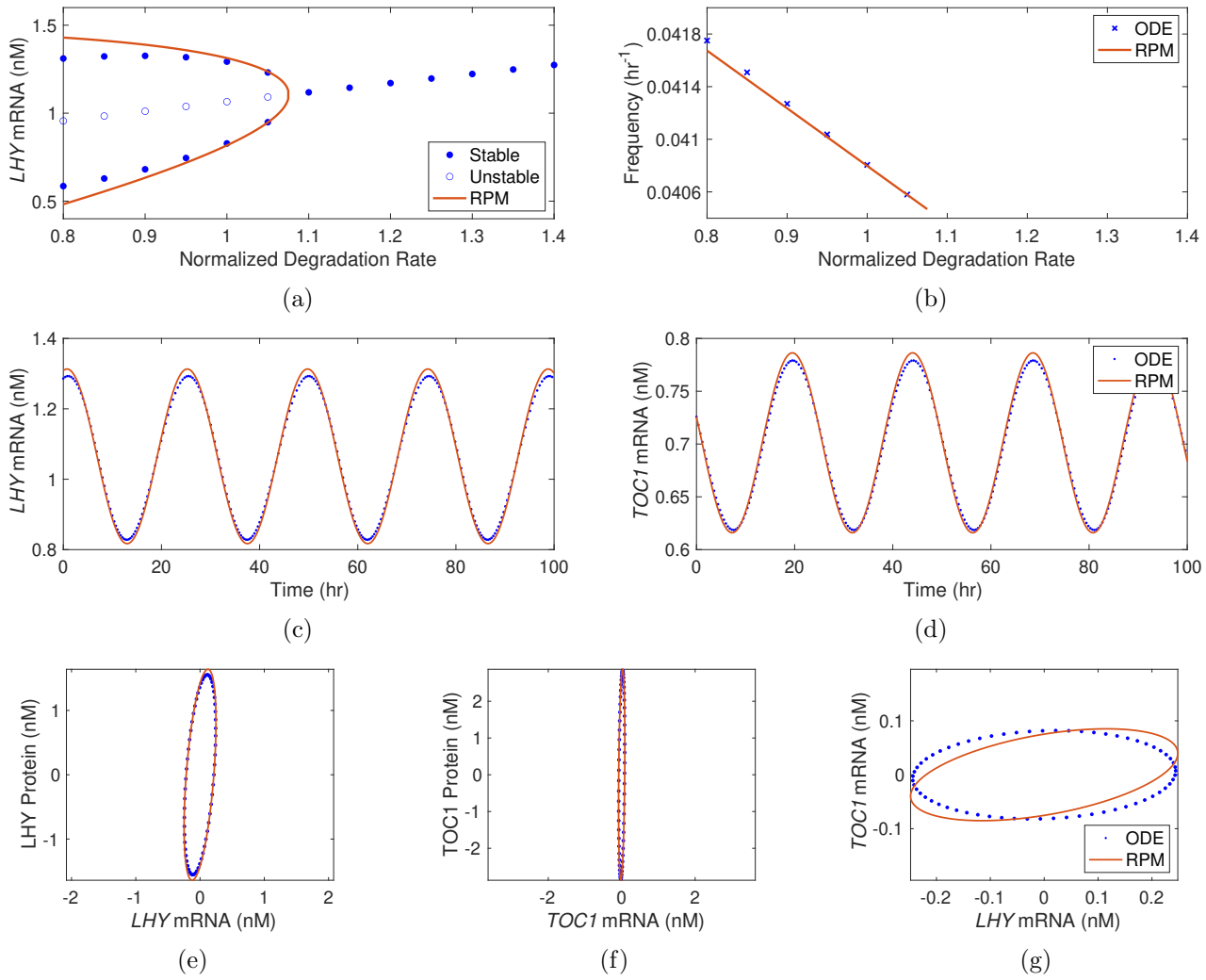

Figure B-1: A supercritical Hopf bifurcation occurs in L2005a model under perpetual illumination. Bifurcation diagrams for (a) concentration of *LHY* mRNA and (b) frequency of oscillation, time series generated from both ODE and RPM for concentrations of (c) *LHY* mRNA and (d) *TOC1* mRNA, and (e) - (g) phase diagrams of pairs of LHY and TOC1 protein in the cytoplasm and *LHY* and *TOC1* mRNA oscillations are shown. The degradation rate in (a) and (b) are normalized so that the biological value given in the original paper is unity. The amplitude of limit cycle oscillation calculated with RPM matches the numerical solution of the system of ODEs with 6.69 percent difference at biological values; and frequency with 0.006 percent difference. As fractions of 2π, the absolute values of differences in phase difference are 0.006 for the pair (*LHY* mRNA, LHY protein), 0.001 for the pair (*TOC1* mRNA, TOC1 protein), and 0.063 for the pair (*LHY* mRNA, *TOC1* mRNA).

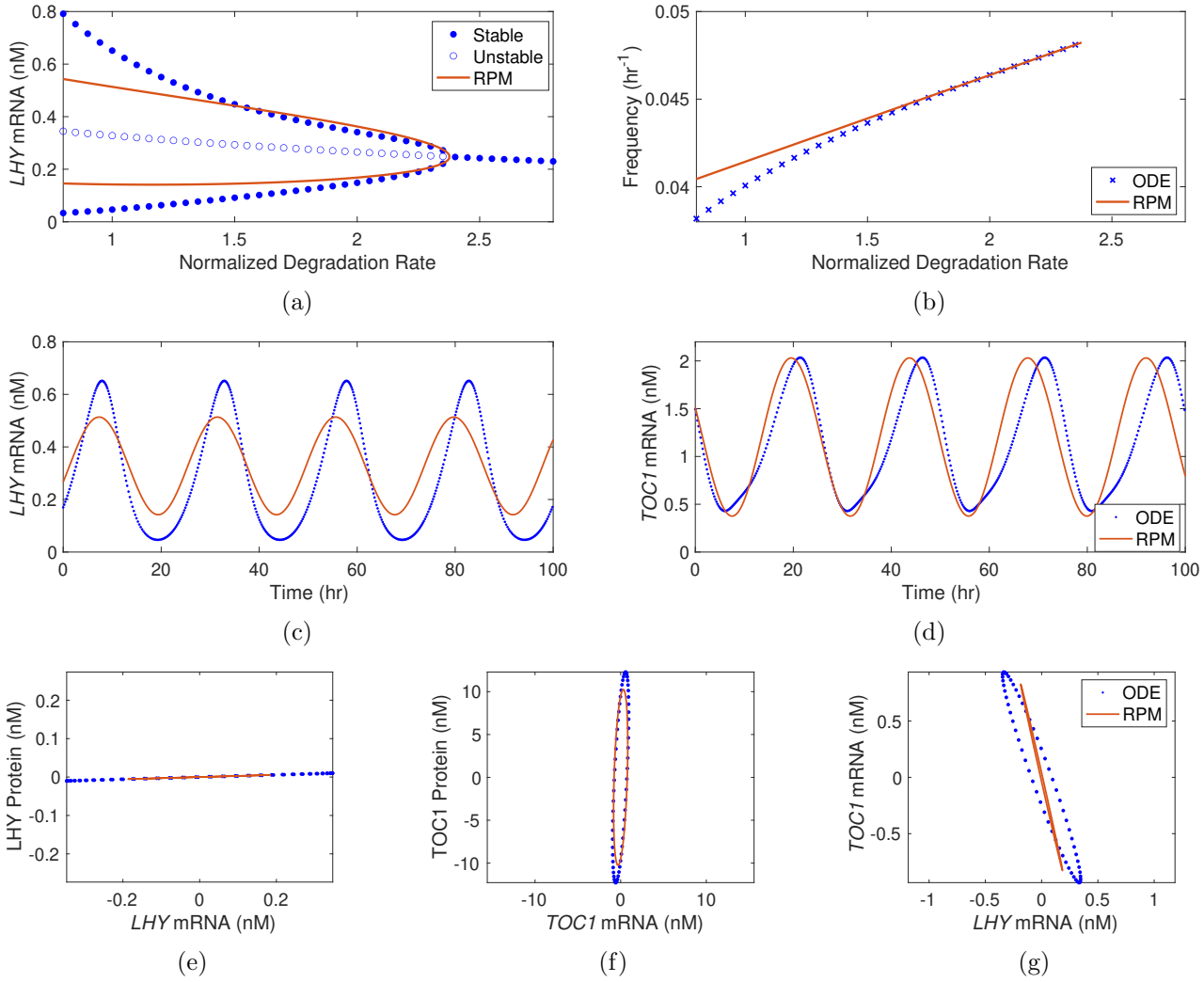

Figure B-2: A supercritical Hopf bifurcation occurs in L2005b model under perpetual illumination. Bifurcation diagrams for (a) concentration of *LHY* mRNA and (b) frequency of oscillation, time series generated from both ODE and RPM for concentrations of (c) *LHY* mRNA and (d) *TOC1* mRNA, and (e) - (g) phase diagrams of pairs of LHY and TOC1 protein in the cytoplasm and *LHY* and *TOC1* mRNA oscillations are shown. The degradation rate in (a) and (b) are normalized so that the biological value given in the original paper is unity. The amplitude of limit cycle oscillation calculated with RPM matches the numerical solution of the system of ODEs with 38.60 percent difference; and frequency with 3.24 percent difference. As fractions of 2π, the absolute values of differences in phase difference are 0.002 for the pair (*LHY* mRNA, LHY protein), 0.045 for the pair (*TOC1* mRNA, TOC1 protein), and 0.035 for the pair (*LHY* mRNA, *TOC1* mRNA).

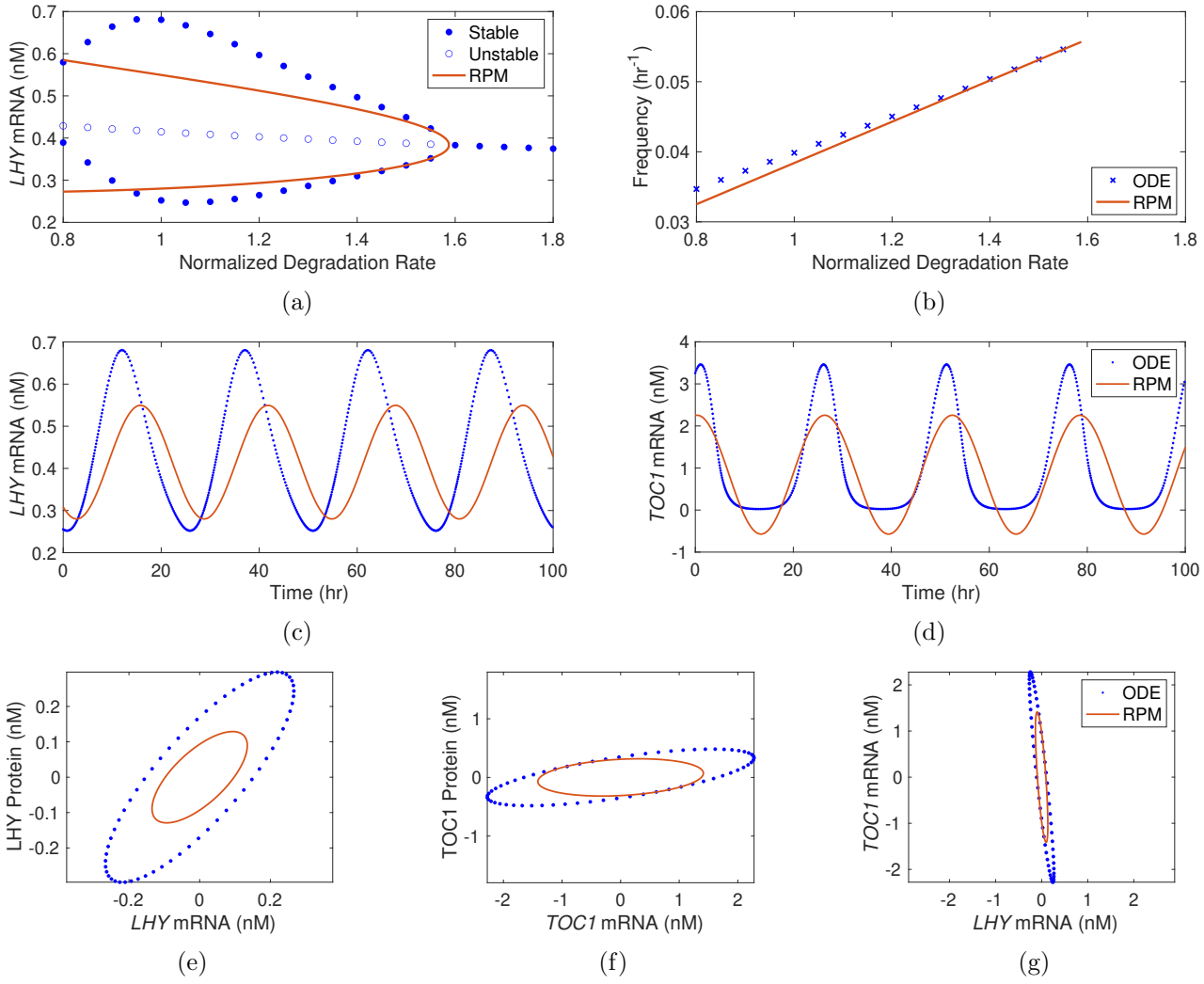

Figure B-3: A supercritical Hopf bifurcation occurs in Z2006 model under perpetual illumination. Bifurcation diagrams for (a) concentration of *LHY* mRNA and (b) frequency of oscillation, time series generated from both ODE and RPM for concentrations of (c) *LHY* mRNA and (d) *TOC1* mRNA, and (e) - (g) phase diagrams of pairs of LHY and TOC1 protein in the cytoplasm and *LHY* and *TOC1* mRNA oscillations are shown. The degradation rate in (a) and (b) are normalized so that the biological value given in the original paper is unity. The amplitude of limit cycle oscillation calculated with RPM matches the numerical solution of the system of ODEs with 37.09 percent difference; and frequency with 3.79 percent difference. As fractions of 2π, the absolute values of differences in phase difference are 0.032 for the pair (*LHY* mRNA, LHY protein), 0.085 for the pair (*TOC1* mRNA, TOC1 protein), and 0.054 for the pair (*LHY* mRNA, *TOC1* mRNA).

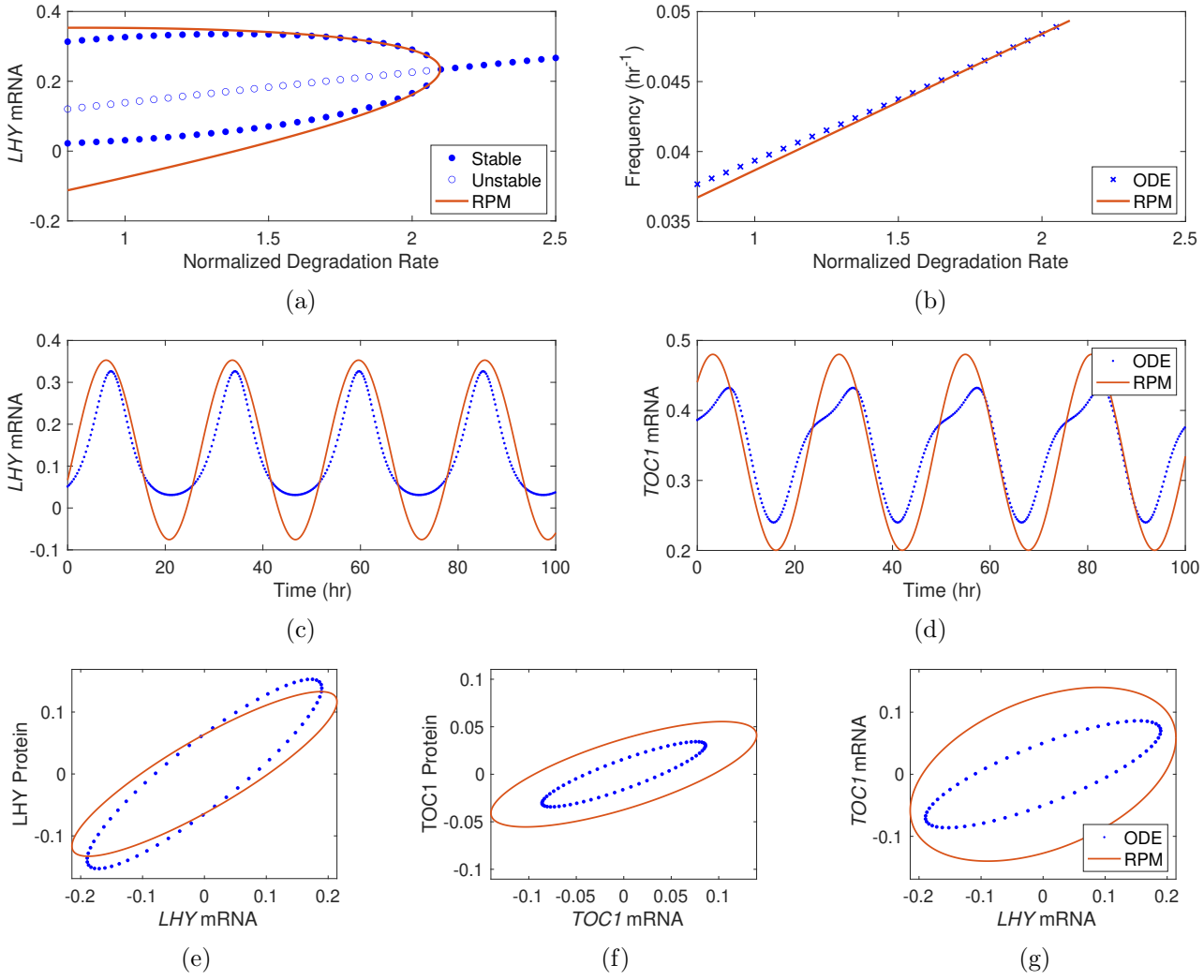

Figure B-4: A supercritical Hopf bifurcation occurs in P2010 model under perpetual illumination. Bifurcation diagrams for (a) concentration of *LHY* mRNA and (b) frequency of oscillation, time series generated from both ODE and RPM for concentrations of (c) *LHY* mRNA and (d) *TOC1* mRNA, and (e) - (g) phase diagrams of pairs of LHY and TOC1 protein in the cytoplasm and *LHY* and *TOC1* mRNA oscillations are shown. The degradation rate in (a) and (b) are normalized so that the biological value given in the original paper is unity. The amplitude of limit cycle oscillation calculated with RPM matches the numerical solution of the system of ODEs with 45.02 percent difference; and frequency with 1.53 percent difference. As fractions of 2π, the absolute values of differences in phase difference are 0.011 for the pair (*LHY* mRNA, LHY protein), 0.041 for the pair (*TOC1* mRNA, TOC1 protein), and 0.082 for the pair (*LHY* mRNA, *TOC1* mRNA).

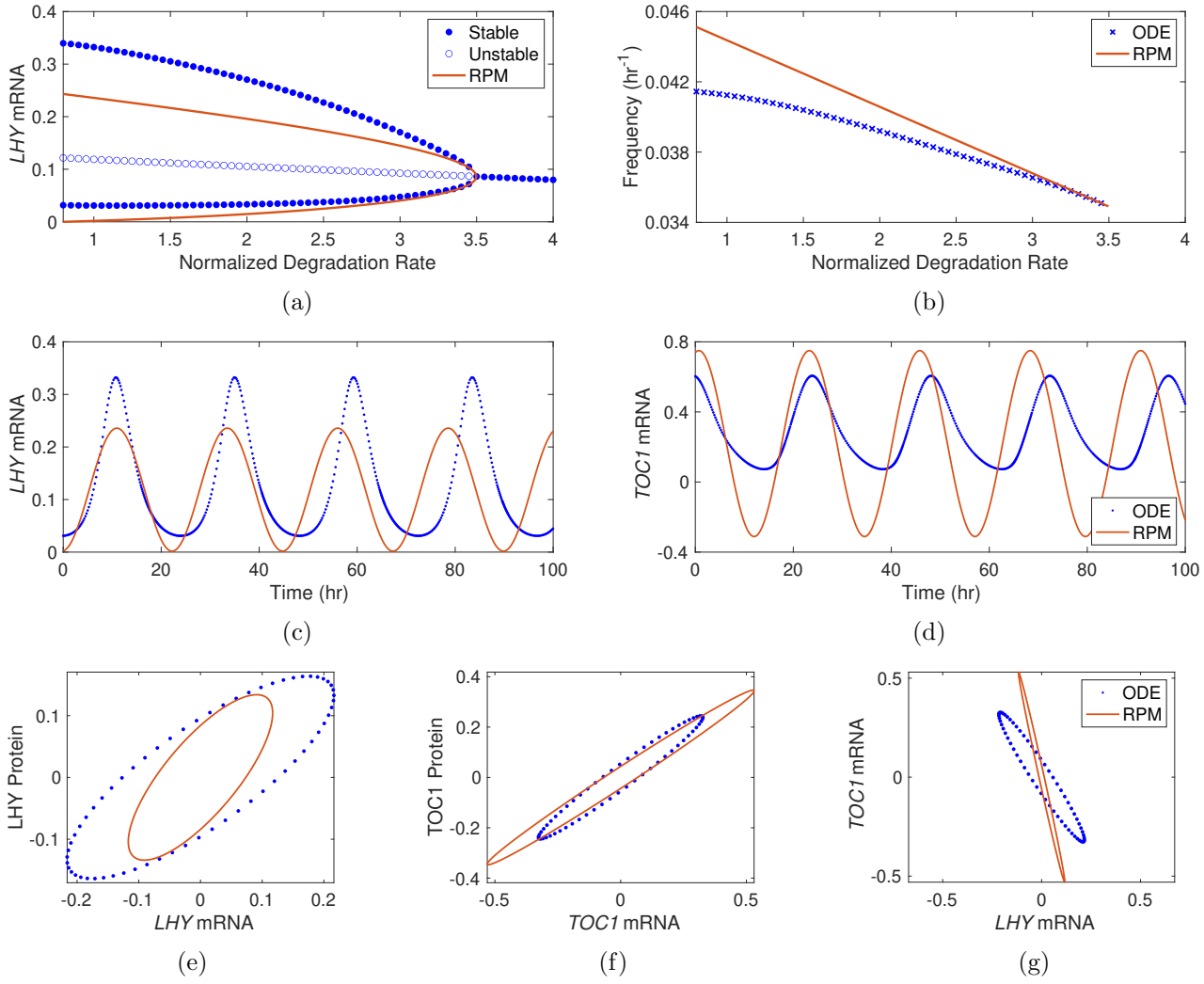

Figure B-5: A supercritical Hopf bifurcation occurs in P2012 model under perpetual illumination. Bifurcation diagrams for (a) concentration of *LHY* mRNA and (b) frequency of oscillation, time series generated from both ODE and RPM for concentrations of (c) *LHY* mRNA and (d) *TOC1* mRNA, and (e) - (g) phase diagrams of pairs of LHY and TOC1 protein in the cytoplasm and *LHY* and *TOC1* mRNA oscillations are shown. The degradation rate in (a) and (b) are normalized so that the biological value given in the original paper is unity. The amplitude of limit cycle oscillation calculated with RPM matches the numerical solution of the system of ODEs with 21.80 percent difference; and frequency with 7.77 percent difference. As fractions of 2π, the absolute values of differences in phase difference are 0.009 for the pair (*LHY* mRNA, LHY protein), 0.016 for the pair (*TOC1* mRNA, TOC1 protein), and 0.024 for the pair (*LHY* mRNA, *TOC1* mRNA).

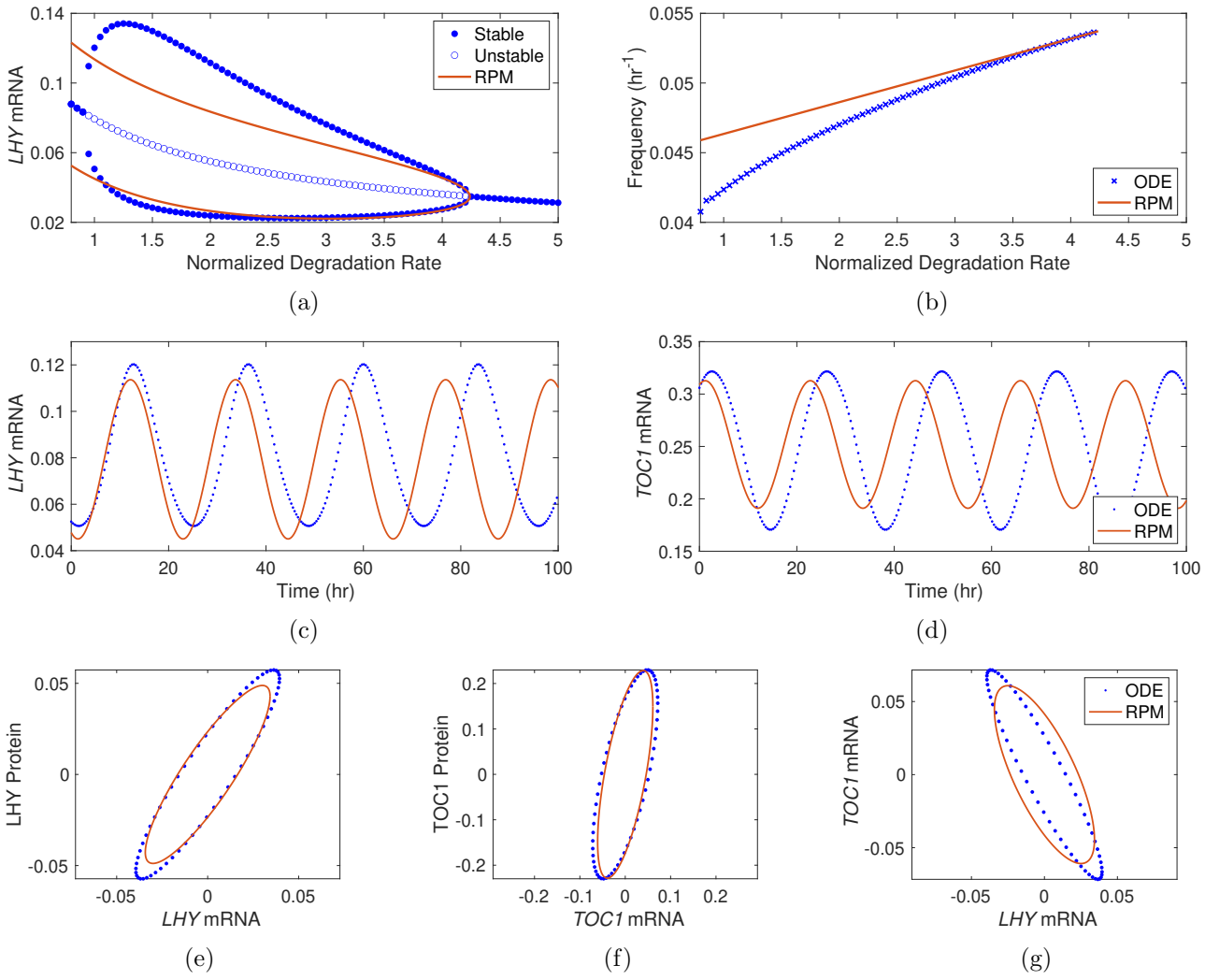

Figure B-6: A supercritical Hopf bifurcation occurs in F2014 model under perpetual illumination. Bifurcation diagrams for (a) concentration of *LHY* mRNA and (b) frequency of oscillation, time series generated from both ODE and RPM for concentrations of (c) *LHY* mRNA and (d) *TOC1* mRNA, and (e) - (g) phase diagrams of pairs of LHY and TOC1 protein in the cytoplasm and *LHY* and *TOC1* mRNA oscillations are shown. The degradation rate in (a) and (b) are normalized so that the biological value given in the original paper is unity. The amplitude of limit cycle oscillation calculated with RPM matches the numerical solution of the system of ODEs with 1.58 percent difference; and frequency with 9.20 percent difference. There is a second Hopf bifurcation near a normalized degradation rate of unity, which is excluded due to our criteria as the subcritical region for this second bifurcation corresponds to lower degradation rate. As fractions of 2π, the absolute values of differences in phase difference are 0.015 for the pair (*LHY* mRNA, LHY protein), 0.006 for the pair (*TOC1* mRNA, TOC1 protein), and 0.059 for the pair (*LHY* mRNA, *TOC1* mRNA).

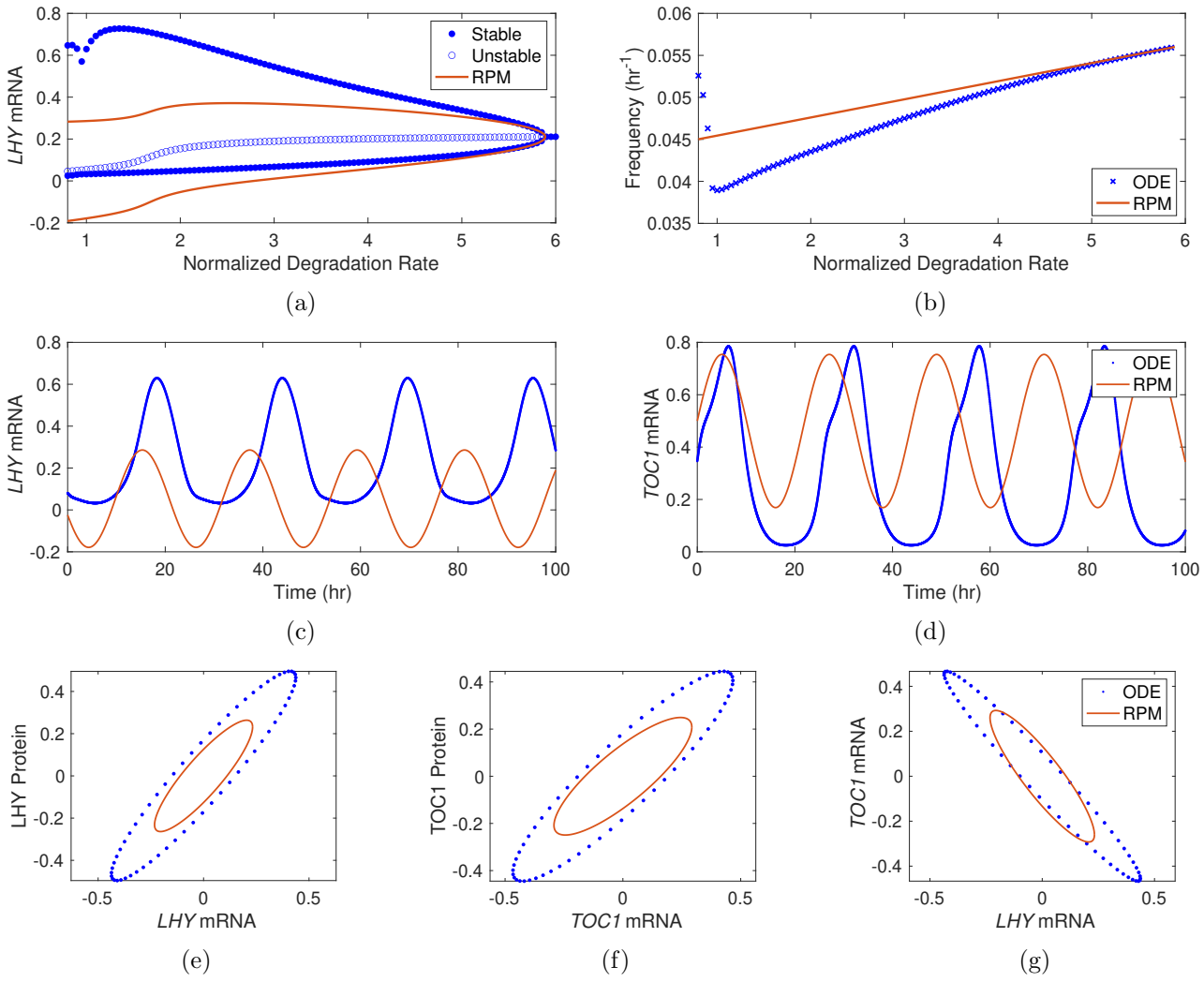

Figure B-7: A supercritical Hopf bifurcation occurs in F2016 model under perpetual illumination. Bifurcation diagrams for (a) concentration of *LHY* mRNA and (b) frequency of oscillation, time series generated from both ODE and RPM for concentrations of (c) *LHY* mRNA and (d) *TOC1* mRNA, and (e) - (g) phase diagrams of pairs of LHY and TOC1 protein in the cytoplasm and *LHY* and *TOC1* mRNA oscillations are shown. The degradation rate in (a) and (b) are normalized so that the biological value given in the original paper is unity. The amplitude of limit cycle oscillation calculated with RPM matches the numerical solution of the system of ODEs with 22.17 percent difference; and frequency with 16.71 percent difference. As fractions of 2π, the absolute values of differences in phase difference are 0.024 for the pair (*LHY* mRNA, LHY protein), 0.026 for the pair (*TOC1* mRNA, TOC1 protein), and 0.039 for the pair (*LHY* mRNA, *TOC1* mRNA).

B.2 Bifurcation Diagrams, Time Series, and Phase Diagrams for Supercritical Models under Perpetual Darkness

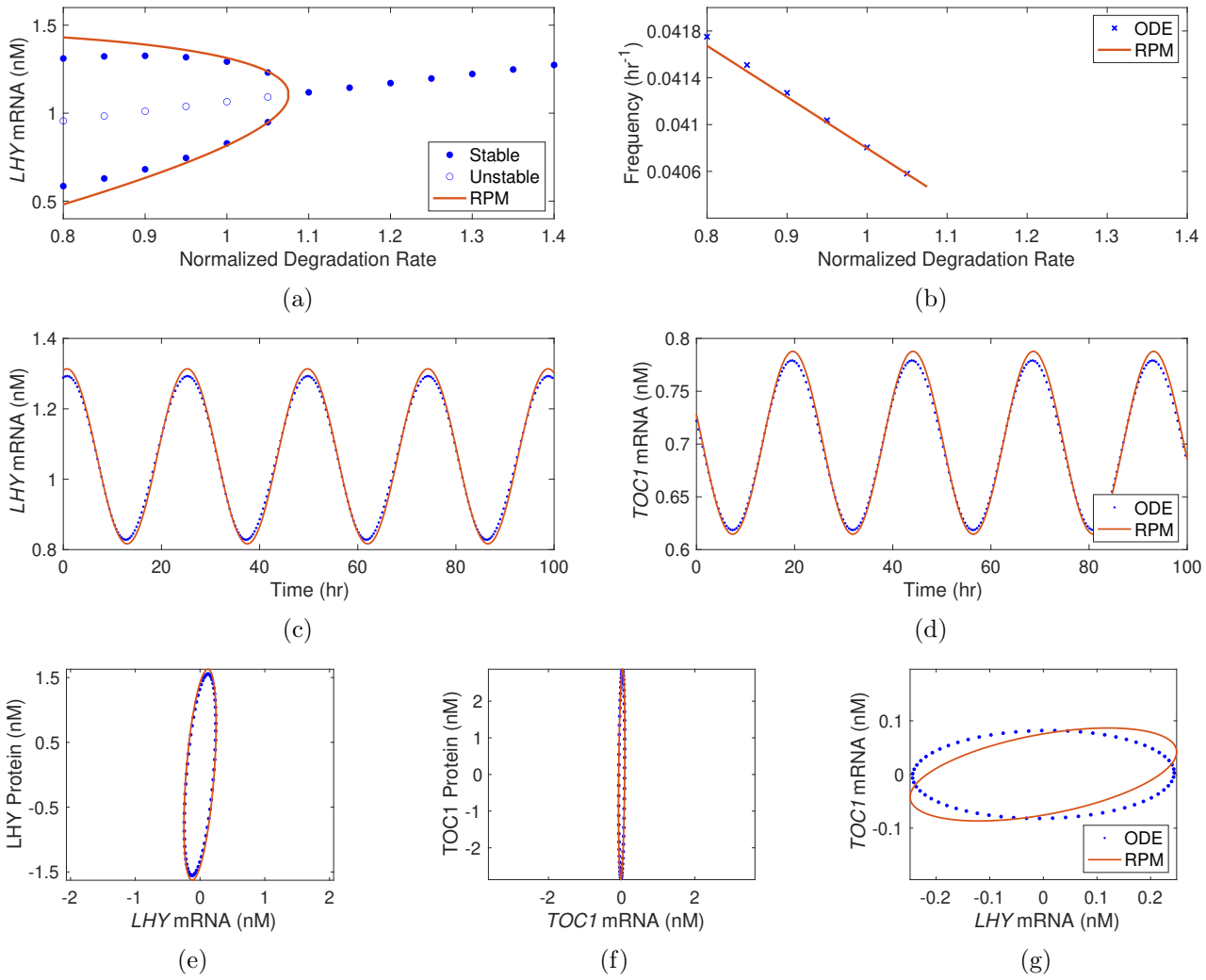

Figure B-8: A supercritical Hopf bifurcation occurs in L2005a model under perpetual darkness. Bifurcation diagrams for (a) concentration of *LHY* mRNA and (b) frequency of oscillation, time series generated from both ODE and RPM for concentrations of (c) *LHY* mRNA and (d) *TOC1* mRNA, and (e) - (g) phase diagrams of pairs of LHY and TOC1 protein in the cytoplasm and *LHY* and *TOC1* mRNA oscillations are shown. The degradation rate in (a) and (b) are normalized so that the biological value given in the original paper is unity. The amplitude of limit cycle oscillation calculated with RPM matches the numerical solution of the system of ODEs with 14.78 percent difference; and frequency with 0.02 percent difference. As fractions of 2π, the absolute values of differences in phase difference are 0.004 for the pair (*LHY* mRNA, LHY protein), 0.011 for the pair (*TOC1* mRNA, TOC1 protein), and 0.074 for the pair (*LHY* mRNA, *TOC1* mRNA).

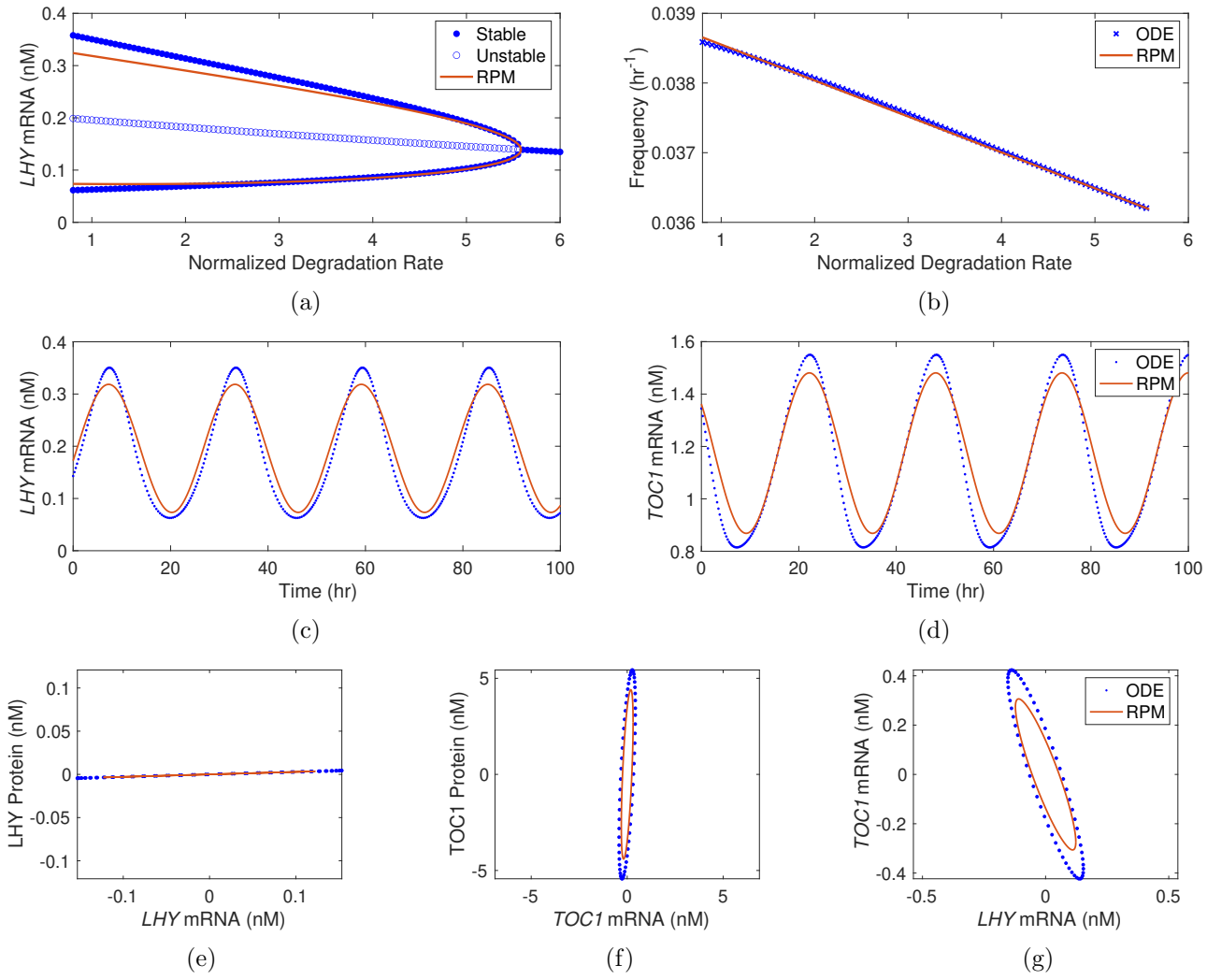

Figure B-9: A supercritical Hopf bifurcation occurs in L2005b model under perpetual darkness. Bifurcation diagrams for (a) concentration of *LHY* mRNA and (b) frequency of oscillation, time series generated from both ODE and RPM for concentrations of (c) *LHY* mRNA and (d) *TOC1* mRNA, and (e) - (g) phase diagrams of pairs of LHY and TOC1 protein in the cytoplasm and *LHY* and *TOC1* mRNA oscillations are shown. The degradation rate in (a) and (b) are normalized so that the biological value given in the original paper is unity. The amplitude of limit cycle oscillation calculated with RPM matches the numerical solution of the system of ODEs with 14.78 percent difference; and frequency with 0.26 percent difference. As fractions of 2π, the absolute values of differences in phase difference are 0.0003 for the pair (*LHY* mRNA, LHY protein), 0.004 for the pair (*TOC1* mRNA, TOC1 protein), and 0.003 for the pair (*LHY* mRNA, *TOC1* mRNA).

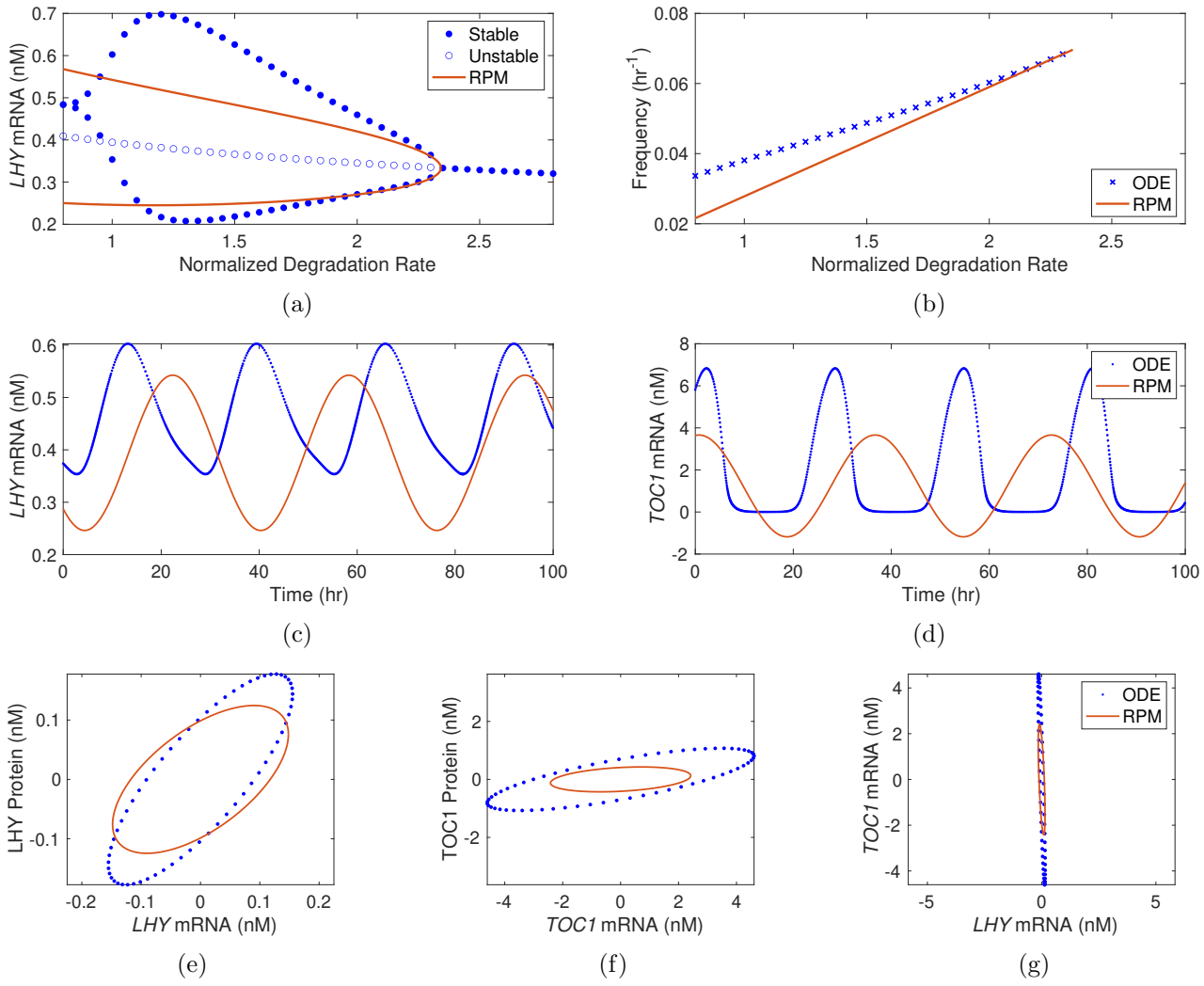

Figure B-10: A supercritical Hopf bifurcation occurs in Z2006 model under perpetual darkness. Bifurcation diagrams for (a) concentration of *LHY* mRNA and (b) frequency of oscillation, time series generated from both ODE and RPM for concentrations of (c) *LHY* mRNA and (d) *TOC1* mRNA, and (e) - (g) phase diagrams of pairs of LHY and TOC1 protein in the cytoplasm and *LHY* and *TOC1* mRNA oscillations are shown. The degradation rate in (a) and (b) are normalized so that the biological value given in the original paper is unity. The amplitude of limit cycle oscillation calculated with RPM matches the numerical solution of the system of ODEs with 19.04 percent difference; and frequency with 27.03 percent difference. As fractions of 2π, the absolute values of differences in phase difference are 0.046 for the pair (*LHY* mRNA, LHY protein), 0.089 for the pair (*TOC1* mRNA, TOC1 protein), and 0.058 for the pair (*LHY* mRNA, *TOC1* mRNA).

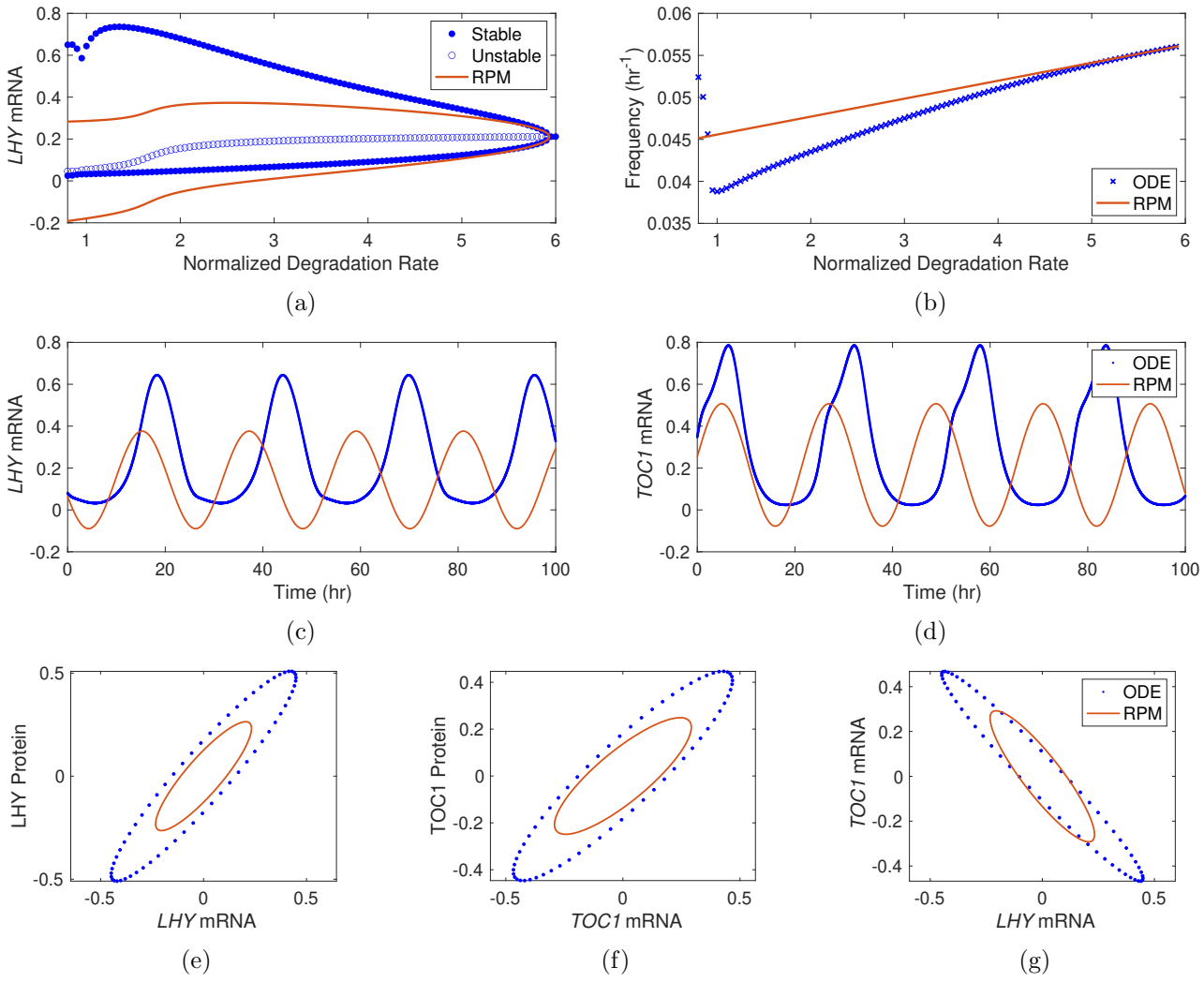

Figure B-11: A supercritical Hopf bifurcation occurs in F2016 model under perpetual darkness. Bifurcation diagrams for (a) concentration of *LHY* mRNA and (b) frequency of oscillation, time series generated from both ODE and RPM for concentrations of (c) *LHY* mRNA and (d) *TOC1* mRNA, and (e) - (g) phase diagrams of pairs of LHY and TOC1 protein in the cytoplasm and *LHY* and *TOC1* mRNA oscillations are shown. The degradation rate in (a) and (b) are normalized so that the biological value given in the original paper is unity. The amplitude of limit cycle oscillation calculated with RPM matches the numerical solution of the system of ODEs with 23.88 percent difference; and frequency with 17.53 percent difference. As fractions of 2π, the absolute values of differences in phase difference are 0.024 for the pair (*LHY* mRNA, LHY protein), 0.026 for the pair (*TOC1* mRNA, TOC1 protein), and 0.039 for the pair (*LHY* mRNA, *TOC1* mRNA).

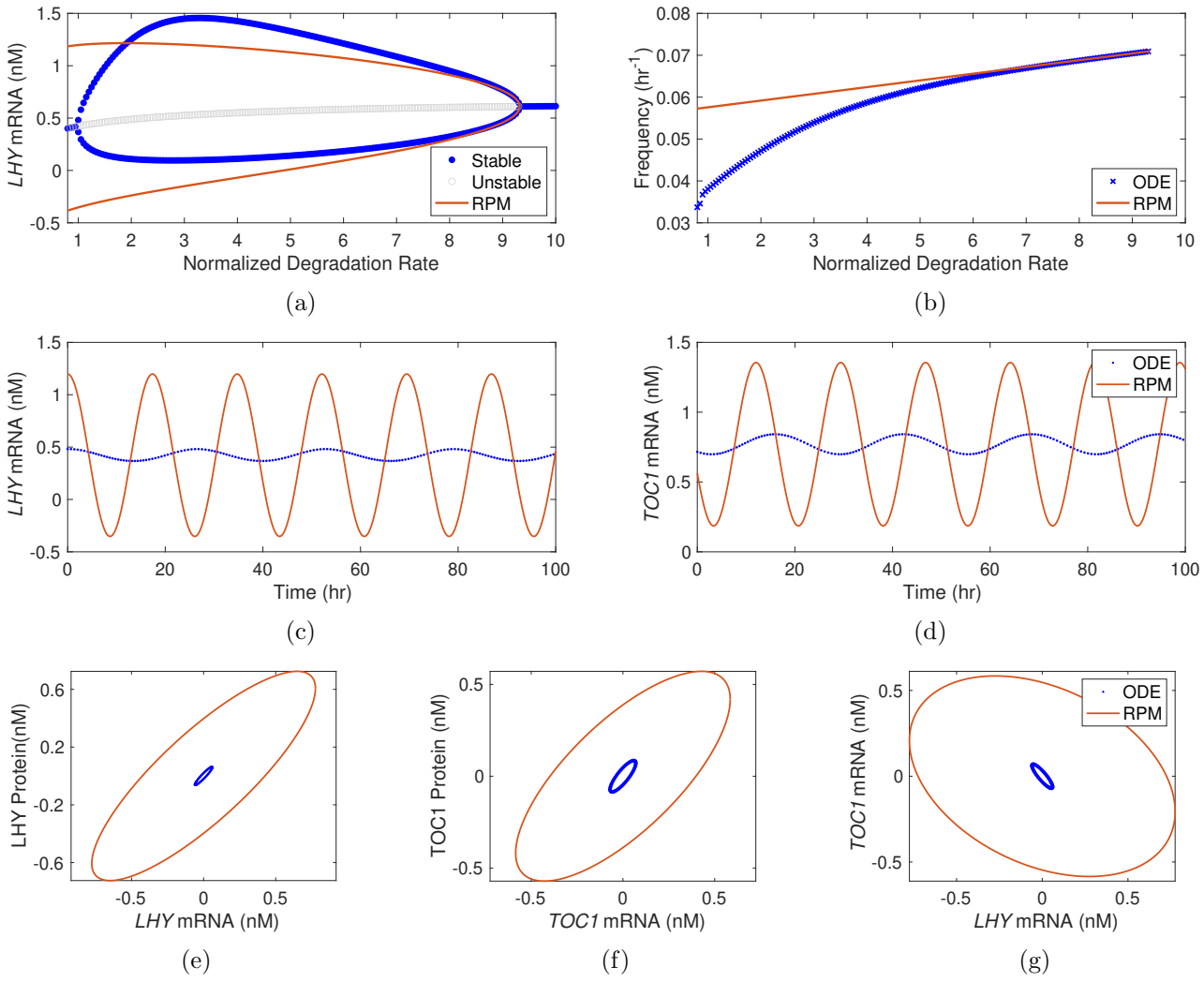

Figure B-12: A supercritical Hopf bifurcation occurs in DC2016 model under perpetual darkness. Bifurcation diagrams for (a) concentration of *LHY* mRNA and (b) frequency of oscillation, time series generated from both ODE and RPM for concentrations of (c) *LHY* mRNA and (d) *TOC1* mRNA, and (e) - (g) phase diagrams of pairs of LHY and TOC1 protein in the cytoplasm and *LHY* and *TOC1* mRNA oscillations are shown. The degradation rate in (a) and (b) are normalized so that the biological value given in the original paper is unity. The amplitude of limit cycle oscillation calculated with RPM matches the numerical solution of the system of ODEs with 1267.28 percent difference; and frequency with 51.58 percent difference. There is a second Hopf bifurcation near a normalized degradation rate of unity, which is excluded due to our criteria as the subcritical region for this second bifurcation corresponds to lower degradation rate. As fractions of 2π, the absolute values of differences in phase difference are 0.039 for the pair (*LHY* mRNA, LHY protein), 0.027 for the pair (*TOC1* mRNA, TOC1 protein), and 0.113 for the pair (*LHY* mRNA, *TOC1* mRNA).

B.3 Asymptotic Amplitude and Frequency of Oscillation of Each Model under Perpetual Illumination

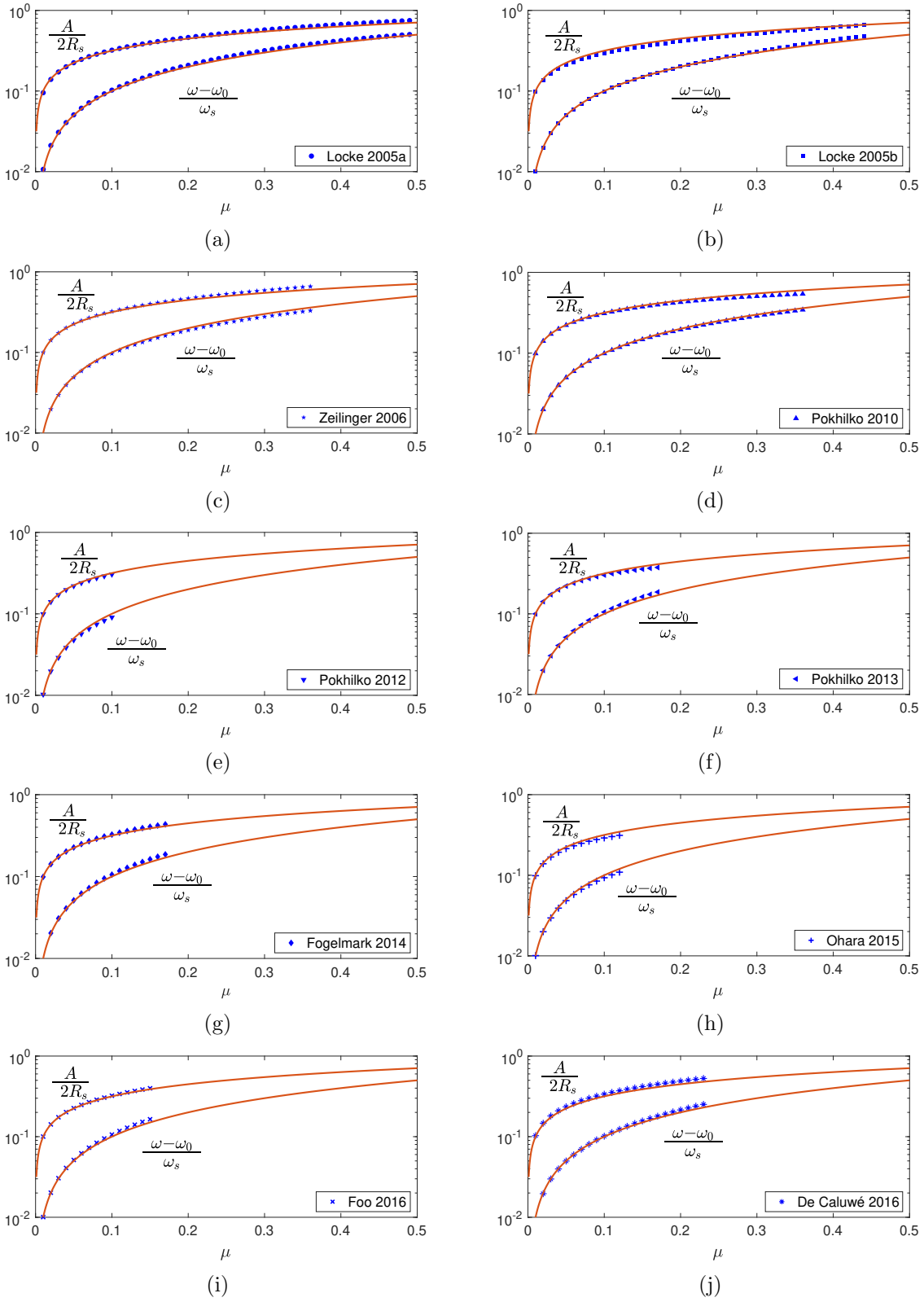

Figure B-13: Amplitude and frequency collapse for each model under perpetual illumination.

B.4 Asymptotic Amplitude and Frequency of Oscillation of Each Model under Perpetual Darkness

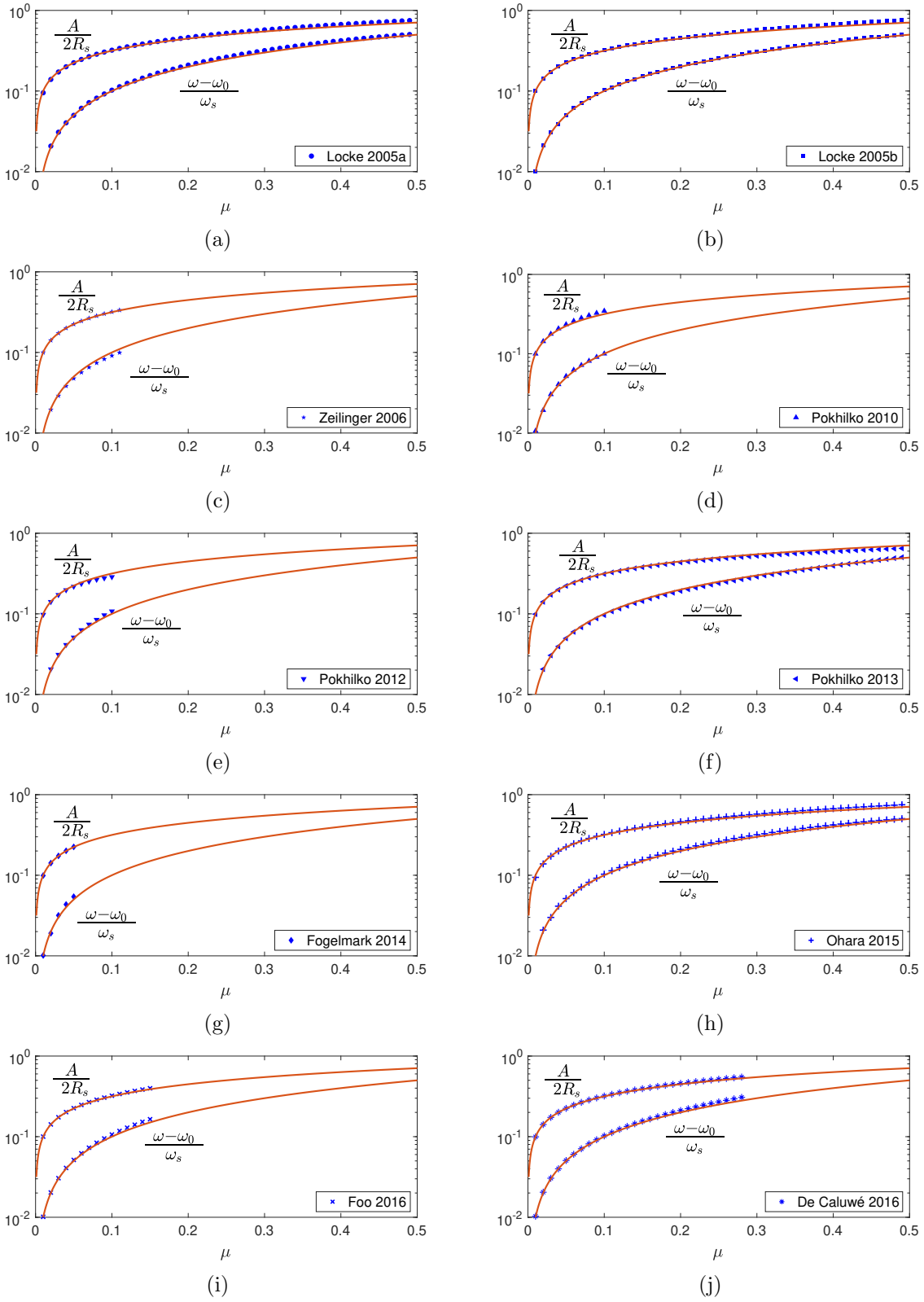

Figure B-14: Amplitude and frequency collapse for each model under perpetual darkness.

B.5 Stuart-Landau Parameter Values under Perpetual Illumination

Model	BP	Scaled By	Optimal Value	Critical Value	ω_0	$g = g' + ig''$	$\lambda_1 = \sigma_1 + i\omega_1$
L2005a	m_2	$TOC1_c$	16.9058	6.2609	0.3013	$0.1686 + 0.1471i$	$0.0022 + 0.0088i$
L2005b	m_1	$TOC1_c$	1.5283	3.6327	0.3031	$0.0003 + 0.0000i$	$0.0041 - 0.0197i$
Z2006	m_{12}	Y_n	5.9504	9.4460	0.3500	$0.0015 + 0.0070i$	$0.0054 - 0.0059i$
P2010	m_3	Y Protein	0.2	0.4195	0.3101	$0.1844 + 0.4475i$	$0.0929 - 0.0807i$
P2012	m_{35}	LUX	0.3	1.0493	0.2193	$0.0573 + 0.0056i$	$0.0656 + 0.0857i$
P2013	m_{15}	LUX	0.7	0.4099	0.2647	$0.0472 + 0.0595i$	$0.0382 - 0.0269i$
F2014	m_1	$PPR7$ mRNA	0.6127	2.5971	0.3375	$0.1259 + 0.0817i$	$0.0131 - 0.0149i$
O2015	m_1	$TOC1_c$	9.3383	9.0593	0.2614	$0.1076 + 0.0817i$	$0.0099 + 0.0206i$
F2016	ϕ_{36}	$PPR7$ mRNA	0.37854	2.2289	0.3519	$0.7441 + 0.3900i$	$0.0215 - 0.0246i$
DC2016	d_7	ELF4/LUX Protein	0.38	0.2232	0.2477	$0.1318 + 0.1077i$	$0.0979 - 0.2052i$

Table B.1: Bifurcation parameters (BP), the chemical species that corresponds to the component in the eigenvectors with the largest modulus (Scaled By), optimal and critical values of the bifurcation parameter for each model, along with important Stuart-Landau parameters. Calculations and simulations are conducted under perpetual illumination.

B.6 Stuart-Landau Parameter Values under Perpetual Darkness

Model	BP	Scaled By	Optimal Value	Critical Value	ω_0	$g = g' + ig''$	$\lambda_1 = \sigma_1 + i\omega_1$
L2005a	m_2	$TOC1_c$	16.9058	6.2609	0.3013	$0.1686 + 0.1471i$	$0.0022 + 0.0088i$
L2005b	m_{13}	$TOC1_c$	0.1347	0.7518	0.2274	$0.0030 - 0.0010i$	$0.0232 + 0.0160i$
Z2006	m_{12}	Y_n	5.9504	13.9347	0.4377	$0.0015 + 0.0086i$	$0.0050 - 0.0035i$
P2010	m_{10}	Y Protein	0.3	0.2751	0.1952	$1.0472 + 0.2216i$	$0.1800 + 0.1757i$
P2012	m_{19}	LUX	0.2	0.0738	0.2225	$0.0691 + 0.0539i$	$0.1013 - 0.5555i$
P2013	m_{15}	LUX	0.7	0.6589	0.2541	$0.0655 + 0.0725i$	$0.0245 + 0.0171i$
F2014	m_{31}	LUX	0.3	0.1017	0.2842	$0.0343 + 0.0411i$	$0.1516 + 0.2601i$
O2015	m_2	$TOC1_c$	16.9058	6.2609	0.3013	$0.1686 + 0.1471i$	$0.0022 + 0.0088i$
F2016	ϕ_{36}	$PPR7$ mRNA	0.37854	2.2453	0.3523	$0.7458 + 0.3953i$	$0.0213 - 0.0242i$
DC2016	k_2	$CCA1/LHY$ mRNA	0.21	1.9574	0.4457	$0.5415 + 0.6186i$	$0.0466 + 0.0051i$

Table B.2: Bifurcation parameters (BP), the chemical species that corresponds to the component in the eigenvectors with the largest modulus (Scaled By), optimal and critical values of the bifurcation parameter for each model, along with important Stuart-Landau parameters. Calculations and simulations are conducted under perpetual darkness.

B.7 Eigenvector Entries under Perpetual Illumination

Chemical Species	L2005a	L2005b	Z2006	P2010
LHY mRNA	-0.0065 - 0.1770i	-0.0060 - 0.0171i	-0.0150 + 0.0116i	-0.1086 - 0.3031i
LHY protein cytoplasm	-0.0406 - 0.2550i	-0.0002 - 0.0005i	-0.0019 + 0.0180i	-0.1496 - 0.1325i
LHY protein nucleus	-0.0658 - 0.1958i	-0.0013 - 0.0027i	-0.0009 + 0.0090i	-0.0759 + 0.0213i
TOC1 mRNA	0.1283 + 0.2329i	0.0302 + 0.0749i	0.1978 - 0.0181i	0.1504 - 0.1471i
TOC1 protein cytoplasm	1.0000 + 0.0000i	1.0000 + 0.0000i	0.0060 - 0.0443i	0.0048 - 0.0832i
TOC1 protein nucleus	0.0088 - 0.1492i	0.0998 - 0.0096i	0.0241 - 0.2542i	-0.0196 - 0.0198i

Table B.3: Eigenvector entries for the mRNA and proteins of $LHY/CCA1$ and $TOC1$ genes under perpetual illumination. For P2010 model, the second and fifth entries are protein (LHY and TOC1 in Pokhilko et al. 2010), and the third and sixth entries are modified protein (LHY_{mod} and TOC1_{mod} in Pokhilko et al. 2010).

Chemical Species	P2012	P2013	F20014	O2015
LHY mRNA	-0.0629 - 0.0056i	-0.0999 - 0.1054i	-0.0347 + 0.0147i	-0.0479 - 0.3371i
LHY protein cytoplasm	-0.0601 + 0.0402i	-0.1464 - 0.0116i	-0.0333 + 0.0422i	-0.0392 - 0.2089i
LHY protein nucleus	-0.0026 + 0.0173i	-0.0275 + 0.0310i		-0.0530 - 0.1568i
TOC1 mRNA	0.2803 - 0.0578i	0.1630 + 0.0013i	0.0630 - 0.0229i	0.1083 + 0.2022i
TOC1 protein cytoplasm	0.1770 - 0.0606i	0.0938 - 0.0310i	0.0887 - 0.2355i	1.0000 + 0.0000i
TOC1 protein nucleus			0.0127 - 0.0313i	0.0061 - 0.1723i

Table B.4: Eigenvector entries for the mRNA and proteins of $LHY/CCA1$ and $TOC1$ genes under perpetual illumination continued. Empty entries are due to different definitions of variables.

Chemical Species	F2016	DC2016
LHY mRNA	-0.1688 + 0.4729i	-0.0813 - 0.3151i
LHY protein	0.0881 + 0.5630i	-0.3003 - 0.4373i
TOC1 mRNA	0.0831 - 0.6266i	0.6043 + 0.4132i
TOC1 protein	-0.3526 - 0.4070i	0.5482 + 0.1650i

Table B.5: Eigenvector entries for the mRNA and proteins of $LHY/CCA1$ and $TOC1$ genes under perpetual illumination continued. F2016 and DC2016 models use only one variable for proteins of LHY and $TOC1$. The $TOC1$ entries represent $PRR5/TOC1$ gene group.

B.8 Eigenvector Entries under Perpetual Darkness

Chemical Species	L2005a	L2005b	Z2006	P2010
LHY mRNA	-0.0065 - 0.1770i	-0.0054 - 0.0273i	-0.0102 + 0.0098i	-0.5879 - 0.2651i
LHY protein cytoplasm	-0.0406 - 0.2550i	-0.0002 - 0.0008i	0.0013 + 0.0118i	-0.4563 + 0.0538i
LHY protein nucleus	-0.0658 - 0.1958i	-0.0013 - 0.0044i	0.0007 + 0.0059i	-0.1291 + 0.1596i
TOC1 mRNA	0.1283 + 0.2329i	0.0426 + 0.0550i	0.2296 - 0.0305i	0.2702 - 0.1906i
TOC1 protein cytoplasm	1.0000 + 0.0000i	1.0000 + 0.0000i	0.0067 - 0.0405i	0.0825 - 0.2191i
TOC1 protein nucleus	0.0088 - 0.1492i	0.0815 - 0.0048i	0.0270 - 0.2324i	-0.0712 - 0.1066i

Table B.6: Eigenvector entries for the mRNA and proteins of $LHY/CCA1$ and $TOC1$ genes under perpetual darkness. For P2010 model, the second and fifth entries are protein (LHY and TOC1 in Pokhilko et al. 2010), and the third and sixth entries are modified protein (LHY_{mod} and TOC1_{mod} in Pokhilko et al. 2010).

Chemical Species	P2012	P2013	F20014	O2015
LHY mRNA	-0.2115 - 0.1598i	-0.0851 - 0.1892i	-0.0966 - 0.0447i	-0.0472 - 0.3212i
LHY protein cytoplasm	-0.1884 - 0.0041i	-0.1261 - 0.0620i	-0.0678 - 0.0001i	-0.0379 - 0.1987i
LHY protein nucleus	-0.0466 + 0.0496i	-0.0420 + 0.0201i		-0.0500 - 0.1490i
TOC1 mRNA	0.1737 + 0.0253i	0.0827 + 0.0256i	0.1067 + 0.0126i	0.1031 + 0.1951i
TOC1 protein cytoplasm	0.0727 - 0.0015i	0.0689 - 0.0083i	0.2552 - 0.1780i	1.0000 + 0.0000i
TOC1 protein nucleus			0.0338 - 0.0228i	0.0035 - 0.1787i

Table B.7: Eigenvector entries for the mRNA and proteins of $LHY/CCA1$ and $TOC1$ genes under perpetual darkness continued. Empty entries are due to different definitions of variables.

Chemical Species	F2016	DC2016
LHY mRNA	-0.1706 + 0.4737i	1.0000 + 0.0000i
LHY protein	0.0871 + 0.5645i	0.7818 - 0.5124i
TOC1 mRNA	0.0835 - 0.6265i	-0.2667 + 0.7053i
TOC1 protein	-0.3524 - 0.4064i	0.2779 + 0.6823i

Table B.8: Eigenvector entries for the mRNA and proteins of $LHY/CCA1$ and $TOC1$ genes under perpetual darkness continued. F2016 and DC2016 models use only one variable for proteins of LHY and $TOC1$. The $TOC1$ entries represent $PRR5/TOC1$ gene group.

B.9 Model Idiosyncrasies

Model	ODE Solver	Comments
L2005a [2]	ode15s	The set of parameter values for optimal solution from Fig. 5 in Locke et al. 2005a is used for obtaining data in figure 3 in the main text and supplementary figures 4-1b, B-13a and B-14a. The set of parameter values for a typical annealed solution from Fig. 4 in Locke et al. 2005a is used for obtaining data in supplementary figures B-1 and B-8. Parameters q_1 and q_2 are used with unit h^{-1}, and p_3 with unit nM/h.
L2005b [4]	ode15s	Model Two (the interlocked feedback look model) is used in our analysis, since it adds an extra loop to Model One as an improvement.
Z2006 [5]	ode15s	$PRR7-PRR9light-Y'$ model is used in our analysis. In $PRR7-PRR9light-Y'$ model, in equation of $\frac{dc_Y^{(m)}}{dt}$, term ${c_L^{(n)}}^{fi}$ is interpreted as ${c_L^{(n)}}^{i}$ as in $PRR7-PRR9-Y$ model.
P2010 [6]	ode15s	Model uses dimensionless chemical levels. L is set to 1 for perpetual illumination, and 0 for perpetual darkness in our analysis.
P2012 [7]	ode15s	Model uses dimensionless chemical levels. L is set to 1 for perpetual illumination, and 0 for perpetual darkness in our analysis. We added $c_{Ltot} = c_L + c_{L\ \mathrm{mod}}$, and interpret c_G in Eqs.(25)(26) as c_{Gc}.
P2013 [8]	ode15s	Use dimensionless chemical levels. L is set to 1 for perpetual illumination, and 0 for perpetual darkness in our analysis. Equations for HY5 and HFR1 proteins are not included since they are only used for optimization of $COP1$ parameters and are decoupled from other equations. We added $c_{Ltot} = c_L + c_{L\ \mathrm{mod}}$. We redefined c_{Gn} to be $c_{Gn} = p_{28}c_{Gc}/(p_{29} + m_{19} + p_{17}c_{E3n})$; and c_{AR} to be $c_{AR} = 0.5 \cdot (A_0 + c^m_{ABAR} + g_{29} - \sqrt{(A_0 + c^m_{ABAR} + g_{29}) + 4A_0c^m_{ABAR}})$.
F2014 [9]	ode15s	Use dimensionless chemical levels. The model is situated very close to another bifurcation at a lower degradation rate value under perpetual illumination. We interpret $c_T n$ in Eq. (18) as c_{Tn}.
O2015 [10]	ode15s	All the Θ terms are set to 1 for perpetual illumination, and 0 for perpetual darkness in our analysis.
F2016 [11]	ode23	Use dimensionless chemical levels. The kernel model is used in our analysis. The indexing and notations of parameters used in code given and the ones in main body of the original paper differs, and we followed the convention in the code provided ($\phi_7 \to \phi_{75}$, $\phi_8 \to \phi_{76}$, $\phi_9 \to \phi_{77}$, and $\phi_n \to \phi_{n-3}$ for $n \geq 10$. $\theta_{144} \to \phi_{71}$, $\theta_{145} \to \phi_{72}$).
DC2016 [12]	ode15s	We did not include the PIF gene, which controls the hypocotyl growth, since this gene is decoupled from the rest of the network and is not of special interests for our purposes. The model is situated very close to another bifurcation at a lower degradation rate value under perpetual darkness. We interpret $[P]_p$ in Eq. (3) as $[P]$; and P in Eq. (9) as the concentration $[P]$.

Table B.9: Details and modifications to each model in our simulations and analysis.

Appendix C

SSA Information for Locke 2005a Model

C.1 Pseudo Chemical Reactions

The 16 pseudo chemical reactions for L2005a model determined using *Law of Mass Action* are:

$$1: \quad L_m \xrightarrow{p_1} L_c + L_m$$
$$2: \quad L_c \xrightarrow{r_1} L_n$$
$$3: \quad L_n \xrightarrow{r_2} L_c$$
$$4: \quad T_c \xrightarrow{r_3} T_n$$
$$5: \quad T_n \xrightarrow{r_4} T_c$$
$$6: \quad T_m \xrightarrow{p_2} T_c + T_m$$
$$7: \quad T_n \xrightarrow{n_1/(g_1+T_n)} L_m + T_n$$
$$8: \quad L_m \xrightarrow{m_1/(k_1+L_m)} X_1$$
$$9: \quad L_c \xrightarrow{m_2/(k_2+L_c)} X_2$$
$$10: \quad L_n \xrightarrow{m_3/(k_3+L_n)} X_3$$
$$11: \quad T_m \xrightarrow{m_4/(k_4+T_m)} X_4$$
$$12: \quad T_c \xrightarrow{m_5/(k_5+T_c)} X_5$$
$$13: \quad T_n \xrightarrow{m_6/(k_6+T_n)} X_6$$
$$14: \quad P_n \xrightarrow{m_7/(k_7+P_n)} X_7$$
$$15: \quad Y_1 \xrightarrow{p'_3} P_n \quad ([Y_1] \cdot p'_3 = p_3)$$
$$16: \quad Y_2 \xrightarrow{n'_2 g_2^2/(g_2^2+L_n^2)} P_n \quad ([Y_2] \cdot n'_2 = n_2)$$

The subscriptions m, c, n stand for the mRNA and proteins in the $c$ytoplasm and $n$ucleus; L and T stand for the $LHY/CCA1$ and $TOC1$ gene; P_n is the light-sensitive protein. The rate constants are associated with transcription (n, g), degradation (m, k), translation (p), and protein transport between nucleus and cytoplasm (r). X and Y are species in the source and sink, whose concentrations and molecule numbers are assumed to be constants.

Notice that in the last two pseudo reactions (15 and 16), we split the value of rate constants into the product of the concentration of Y_i and a new rate constant. This split is arbitrary, and does not affect the simulation results. In our simulation, the values of Y_i are set to 1, so the new-defined rate constants are the same as the original rate constants.

C.2 Particle Number Change due to Reactions

$$\text{Channels} = \begin{bmatrix} 0 & 0 & 0 & 0 & 0 & 0 & 1 & -1 & 0 & 0 & 0 & 0 & 0 & 0 & 0 & 0 \\ 1 & -1 & 1 & 0 & 0 & 0 & 0 & 0 & -1 & 0 & 0 & 0 & 0 & 0 & 0 & 0 \\ 0 & 1 & -1 & 0 & 0 & 0 & 0 & 0 & 0 & -1 & 0 & 0 & 0 & 0 & 0 & 0 \\ 0 & 0 & 0 & 0 & 0 & 0 & 0 & 0 & 0 & 0 & -1 & 0 & 0 & 0 & 0 & 1 \\ 0 & 0 & 0 & -1 & 1 & 1 & 0 & 0 & 0 & 0 & 0 & -1 & 0 & 0 & 0 & 0 \\ 0 & 0 & 0 & 1 & -1 & 0 & 0 & 0 & 0 & 0 & 0 & 0 & -1 & 0 & 0 & 0 \\ 0 & 0 & 0 & 0 & 0 & 0 & 0 & 0 & 0 & 0 & 0 & 0 & 0 & -1 & 1 & 0 \end{bmatrix} \tag{C.1}$$

Each column corresponds to a reaction in Section C.1 in the same order. The first seven columns refer to reactions between different chemicals (1-7); the following seven columns capture the degradation of the seven chemical species (8-14); the last two columns are reactions through which certain species entering the system (15-16). From top down, each roll corresponds to a chemical species in the system in the following order: $L_m, L_c, L_n, T_m, T_c, T_n, P_n$.